Author(s)

Lagrangian Computation of Dispersed Turbulent Flows: A Primer

SPIN Springer's internal project number, if known

– Monograph –

August 26, 2003

Springer
Berlin Heidelberg NewYork
HongKong London
Milan Paris Tokyo

Your dedication goes here

Preface

Here come the golden words

place(s),
month year

First name Surname
First name Surname

Contents

1

Introduction

Your text goes here. Separate text sections with the standard LaTeX sectioning commands.

1.1 Applications

1.2 Problems

1.3 Outline

2

Particle dynamics

2.1 Generalities

— NOTA DEL PROF.: gran parte di queste "Generalities" vanno messe in capitoloi iniziale

- Lagrangian approach
  Every particle trajectory is obtained by time-integration of the equation

$$\frac{d}{dt}(m_p \mathbf{v}_p) = \mathbf{F} \tag{2.1}$$

- Advantages of Lagrangian approach
  - *??? more detailed description of particles behaviour (respect to an eulerian approach)*
- Disadvantages of Lagrangian approach
  - Computational costs: lagrangian approached has been only recently used because of its great computational costs (due to the fact that realistic simulations have to compute large number of particles)
  - *??? mettere esempi numerici di costi computazionali*
- Simplifying hypothesis
  Common simplifying hypothesis are:
  - constant mass

$$m_p(d\mathbf{v}_p/dt) = \mathbf{F} \tag{2.2}$$

  - spherical particles (no need to consider particle *orientation*)
  - incompressible flow
  - one-way coupling
  - simplified models on $\mathbf{F}$ = force acting on a particle
    (you have to know the relative importance between the different forces, that will be later described)

2.2 Forces acting on a particle

Two kinds of forces act on a particle moving in a fluid:

$$\mathbf{F} = \mathbf{F_S} + \mathbf{F_B} \tag{2.3}$$

where $\mathbf{F}_S$ are *surface forces*, exerted by the surrounding fluid and $\mathbf{F}_B$ are *body forces*, due to other external agents (e.g. gravity, electrical forces, ...).

Only gravity effects is considered in the body forces term

$$\mathbf{F_B} = \mathbf{F_{grav}} \tag{2.4}$$

where $\mathbf{F}_{grav}$ is the gravity force acting on the particle (see section 2.2.1).

The surface force exerted on a particle by the surrounding fluid should be calculated as $\mathbf{F_S} = \int_{\mathbf{S_p}} \sigma \cdot \mathbf{n}\, \mathbf{dS_p}$ where S_p is particle surface, $\mathbf{n}$ the *outward versor ???* normal to S_p and σ the *fluid stress tensor???* ($\sigma_{ij} = -p\delta_{ij} + \nu\, \partial u_i/\partial x_j$).

This metod requires a detailed knowledge of the flow field in the proximity of the particle (in order to calculate the integral of fluid stress tensor on particle surface). This involves prohibitive computational costs when we want to track a swarm of particles; so the term $\mathbf{F}_S$ has to be modeled. The terms proposed by Maxey and Riley [**?**] are:

$$\mathbf{F_S} = \mathbf{F_{drag}} + \mathbf{F_{pres}} + \mathbf{F_{bouy}} + \mathbf{F_{lift}} + \mathbf{F_{addm}} + \mathbf{F_{bass}} \tag{2.5}$$

where the right-hand-side (RHS) terms represent respectively drag, pressure gradient, buoyancy, lift, added mass and Basset force. These terms are modeled as functions of the physical properties of particles and fluid and of velocity and pressure field of the *undisturbed* flow (i.e. the flow doesn't consider the presence of the particle). In the following sections, if not explicitly said, we will refer to the undisturbed velocity ($\mathbf{u}$) and pressure (p) flow fields.

2.2.1 Gravity force

A particle located in a gravitational field $\mathbf{g}$ is subjected to a gravitational force

$$\mathbf{F}_{grav} = m_p \mathbf{g} \tag{2.6}$$

where the particle mass m_p is, for spherical particles,

$$m_p = \rho_p\, V_p = \rho_p\, \frac{\pi\, d_p^3}{6} \tag{2.7}$$

where ρ_p is particle density, V_p particle volume and d_p particle diameter.

In many practical applications the gravitational field can be considered constant and its value set to $|\mathbf{g}| = 9.81\ m\ s^{-2}$.

2.2.2 Drag force

Drag force can be expressed (see [?]) as:

$$\mathbf{F_{drag}} = \frac{\mathbf{1}}{\mathbf{2}} \mathbf{C_D}\ \rho\ \mathbf{A_f}\ \ |\mathbf{u} - \mathbf{v_p}|\ (\mathbf{u} - \mathbf{v_p}) \tag{2.8}$$

where $\mathbf{u} - \mathbf{v_p}$ is the relative velocity between the fluid and the particle ($\mathbf{u}$ is the fluid velocity in the position occupied by the particle), C_D is the drag coefficient (described in the following), ρ the fluid density and A_f the frontal area of the particle (i.e. the area of the region obtained projecting the particle onto a plane orthogonal to the relative velocity).

Equation 2.8 describes a *steady* drag force; this means that the model is referred to a situation in which:

- the undisturbed flow around the particle presents both a uniform pressure field and a uniform velocity field
- there is no acceleration of the relative velocity between particle and fluid

Drag coefficient

The coefficient C_D is a dimensionless parameter that accounts for the fact that the drag force depends on the way in which the flow is locally modified while passing past the particle.

The dimensionless parameter that characterize the flow on a spherical particle is the particle Reynolds number

$$Re_p = \frac{d_p\,|\mathbf{u} - \mathbf{v_p}|}{\nu} \tag{2.9}$$

where d_p is the particle diameter, $\mathbf{u} - \mathbf{v_p}$ is the relative velocity between the undisturbed fluid and the particle and ν is the fluid kinematic viscosity.

The flow is laminar for low values of Reynolds number; increasing Re_p the separation of the laminar boundary layer and the formation of a turbulent wake can be observed (see [?]). These phenomena change the drag exerted by the fluid.

Then the factor C_D depends on Re_p

$$C_D = C_D(Re_p) \tag{2.10}$$

For nonrotating spherical particle this function is known as the *standard drag curve* and has been experimentally obtained. This curve is shown in figure 2.1

In figure 2.1 it can be observed that particles with non-spherical shape show different behaviours of the coefficient C_D. Moreover, when the spherical simmetry is lost, different curves of $C_D(Re_p)$ are obtained for different directions of the relative velocity $\mathbf{u} - \mathbf{v_p}$.

Other parameters that can influence the drag coefficient are the Mach number and the turbulence level (see [?]).

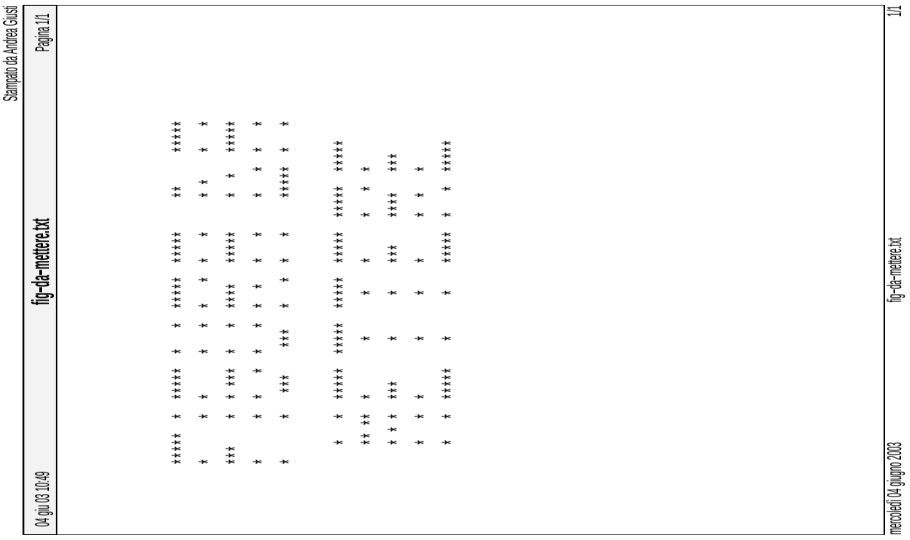

Fig. 2.1. Curves of the drag coefficient C_D for particles of different shape: a) spheres b) cylinders d) disks

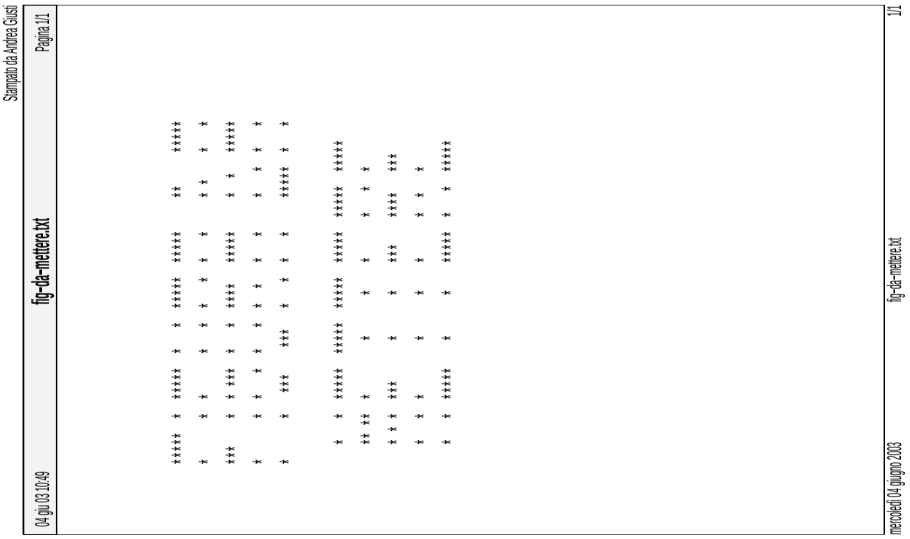

Fig. 2.2. Analytical approximations of the function $C_D = C_D(Re_p)$ for spherical particles

Figure 2.2 shows some analytical approximations of the *standard drag curve* for spherical particles. These analytical expression are listed in the following:

- for $Re_p < 1$ (Stokes flow) the study of a creeping flow past a sphere (see ???) gives the drag force

$$\mathbf{F}_{drag} = 3\ \pi\ \mu\ d_p\ |\mathbf{u} - \mathbf{v_p}| \tag{2.11}$$

and the drag coefficient results

$$C_D = \frac{24}{Re_p} \tag{2.12}$$

- for $1 < Re_p < 5$ the Oseen correction gives

$$C_D = \frac{24}{Re_p}\left(1 + \frac{3}{16}Re_p\right) \tag{2.13}$$

- for $1 < Re_p < 750$ the hypothesis of creeping flow is no more valid and the flow begins ($Re_p = 100$) to separate from the sphere (in the downstream side); this creates a pressure reduction behind the sphere and an increasing factor f is defined to correct the drag respect to valued predicted by Stokes law:

$$C_D = \frac{24}{Re_p}\ f \tag{2.14}$$

The Schiller, Naumann (1933) correlation for f is

$$f = \left(1 + 0.15 Re_p^{0.687}\right) \tag{2.15}$$

??? METTERE ANCHE CORRELAZIONI DI PUTNAM e di CLIFT,GAUVIN - vedi Crowe [**?**], pag.71, eq.(4.52),(4.53)???

- for $750 < Re_p < 3 \cdot 10^5$ (Newton's regime) the drag coefficient has an almost constant value

$$C_D = 0.45 \tag{2.16}$$

- for $Re_p > 3 \cdot 10^5$ (critical Reynolds number) a sharp decrease of drag coefficient is observed. This is due to the fact that the boundary layers become turbulent and the separation point is moved towards the downward side of the sphere; the low pressure zone is then reduced and the drag decreases.
??? CI SONO FORMULE IN QUESTO REGIME ???

Particle characteristic time

Considering the equation of motion of a spherical particle subjected only to a drag force in the hypothesis of Stokes regime, from equations 2.2, 2.8, 2.12, 2.9, we have:

$$\frac{d\mathbf{v}_p}{dt} = \frac{\mathbf{u} - \mathbf{v}_p}{\tau_p} \tag{2.17}$$

where τ_p is the particle characteristic time defined as

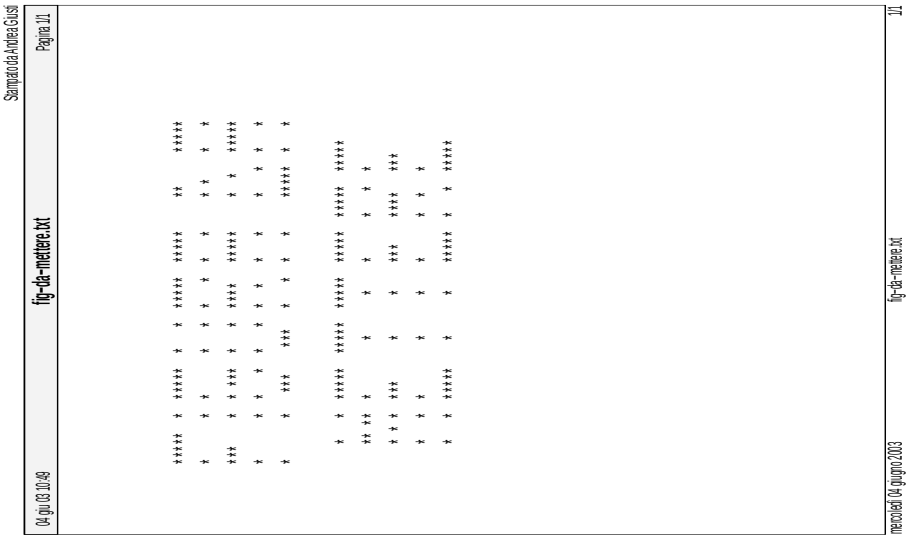

Fig. 2.3. Variation of the velocity of a particle dragged by a fluid at velocity U.

$$\tau_p = \frac{d_p^2 \quad \rho_p}{18 \ \nu \quad \rho} \tag{2.18}$$

The particle characteristic time is a measure of the *inertia* of the particle. Greater or heavier particles have a grater τ_p; this means that longer time is required to the particle to change its velocity when subjected to a drag force.

Example: consider a particle with initial velocity equal to zero ($v_p(t = 0) = 0$); at time $t = 0$ the particle is overwhelmed by a fluid with velocity U; calculate the variation of the particle velocity in time $v_p(t)$ in the hypothesis of Stokes regime.

Solution: the solution of equation 2.17, with $u = U$ constant and with $v_p(t = 0) = 0$, is:

$$v_p(t) = U \left(1 - exp\frac{t}{\tau_p}\right) \tag{2.19}$$

From figure 2.3 we can observe that at the instant $t = \tau_p$ the particle has reached a velocity equal to $v_p(t = \tau_p) = 0.632 \ U$

Stokes-law correction for droplets

Equation 2.12 is valid for solid spheres. Hadamard-Rybczynski generalized this formula to the case of liquid spherical particles (still in the Stokes hypothesis $Re_p < 1$):

$$C_D = \frac{24}{Re_p}\left(\frac{1+\frac{2}{3}\overline{\mu}}{1+\overline{\mu}}\right) \tag{2.20}$$

where $\overline{\mu} = \mu_{carrier}/\mu_{particle}$. In the limit $\overline{\mu} \to 0$ fluid particle behaves as a solid one and eq.(2.12) is obtained; for $\overline{\mu} \to \infty$ the drag coefficient is $C_D = 16/Re_p$. The difference with the solid particles is due to the fact that no-slip conditions on particle surface are no more verified, since shear stresses acting on fluid particle induce internal motions. *??? - il Crowe mette un ref. a Clift et al., 1978 - ???*

??? - e per i casi fuori regime di Stokes ???

Stokes-law correction for nonuniform fields

When the flow velocity field is not uniform, eq.(2.11) can be modified by adding the *Faxen term* (see [**?**]):

$$\mathbf{F}_{drag} = 3\,\pi\,\mu\,d_p\,|\mathbf{u}-\mathbf{v_p}| + \mu\,\pi\,\frac{d_p^3}{8}\,\nabla^2\mathbf{u} \tag{2.21}$$

The modification to the drag force due to the Faxen term depends on the ratio of particle diameter d_p and a characteristic length l of the flow field (e.g. radius of curvature of the velocity distribution):

$$\frac{F_{Faxen}}{F_{Stokes}} \sim \left(\frac{d_p}{l}\right)^2 \tag{2.22}$$

Settling velocity

Heavy particle in a still fluid ($\mathbf{u}$): - gravity force tends to accelerate the particle in downward direction - increasing the particle downward velocity the upward drag force increases - when the drag and the gravity forces have the same value particle downward velocity keeps constant to a value $\mathbf{v_S}$ named *settling velocity*

The value of $\mathbf{v_S}$ can be calculated imposing that $|\mathbf{F_{drag}}| = |\mathbf{F_{grav}}|$; from equations 2.6, 2.14, 2.9 and recalling the definition 2.18 of the characteristic time of the particle, we have:

$$\mathbf{v_S} = \frac{\tau_\mathbf{p}}{\mathbf{f}}\,\mathbf{g} \tag{2.23}$$

??? considerare anche la buoyancy (ancora da definire)

Correction next to the wall

??? - mettere formule articolo Pan,Banerjee (see [**?**])

??? - cosa "sostituiscono" tali correzioni? un gradiente di pressione? se si', non devo usare tali correzioni se considero il termine legato al gradiente di pressione?

2.2.3 Buoyancy force and pressure gradient

When the fluid around a particle has a non-uniform pressure distribution, a net force exerted by the fluid on the particle arise from the integral $\mathbf{F_{p,tot}} = \int_{\mathbf{S_p}} \mathbf{-p_{tot}\ n\ dS_p}$; from the divergence theorem the integral can be written as

$$\mathbf{F_{p,tot}} = \int_{\mathbf{V_p}} \mathbf{-\nabla p_{tot}\ dV_p} \tag{2.24}$$

where V_p is the volume filled by the particle.

The term p_{tot} refers to the effective pressure of the fluid; this is usually splitted in two terms:

$$p_{tot} = p + p_{hydr} \tag{2.25}$$

The hydrostatic pressure is the pressure that arise in a still fluid owing to the gravity effects: $p_{hydr} = p_{hydr,0} - \rho g y$ where $p_{hydr,0}$ is a reference pressure, ρ the fluid density, g the gravitational acceleration and y a vertical coordinate (with positive direction opposite to $\mathbf{g}$).

In many simulations, the pressure field is described in term of relative pressure $p = p_{tot} - p_{hydr}$ (it is possible to eliminate the gravitational term from Navier-stokes equations). In the following we will refer to this relative pressure p.

Pressure gradient term

The term $\mathbf{F_{pres}}$ in equation 2.5 is the force due to the pressure p. Substituting p to p_{tot} in equation 2.24 and assuming that the gradient of the undisturbed pressure field is constant in the volume V_p, we obtain

$$\mathbf{F_{pres}} = \mathbf{-\nabla p\ V_p} \tag{2.26}$$

??? METTERE QUANDO QUESTA IPOTESI DI CONSIDERARE ∇p COSTANTE SU V_p E' VEROSIMILE

??? METTERE QUANDO F_pres E' IMPORTANTE

??? IN Maxey-Riley CONSIDERA DIVERSE FORME DI TERMINE DI GRADIENTE DI PRESSIONE (questa copiata dal Crowe é analoga (a meno di un segno ???) a quella dell'eq. di Corrsin-Lumley (che é all'inizio dell'art. Maxey-Riley))

Buoyancy force

The term $\mathbf{F_{buoy}}$ in equation 2.5 is the force due to the hydrostatic pressure p_{hydr}. Substituting p_{hydr} to p_{tot} in equation 2.24 and having $\nabla p_{hydr} = -\rho\ \mathbf{g}$ we obtain

$$\mathbf{F_{buoy}} = \mathbf{-\rho\ g\ V_p} \tag{2.27}$$

The sum of the term $\mathbf{F_{buoy}}$ and the gravity force $\mathbf{F_{grav}}$ (see equation 2.6) results

$$\mathbf{F_{grav}} + \mathbf{F_{buoy}} = \mathbf{m_p} \left(1 - \frac{\rho}{\rho_\mathbf{p}}\right) \mathbf{g} \tag{2.28}$$

The total effect of these two terms is a force oriented in the same or in the opposite direction of $\mathbf{g}$ respectively if particles are heavier ($\rho_p > \rho$) or lighter ($\rho_p < \rho$) than the fluid.

2.2.4 Lift force

The drag force acts in a direction parallel to the relative velocity between particle and fluid ($\mathbf{u} - \mathbf{v}_p$); particles can be also subjected to a force acting in a direction orthogonal to $\mathbf{u} - \mathbf{v}_p$. This force is called (using an ???aeronautical terminology???) *lift*. The principle is the same that *lifts* the airplanes: the air flowing through the wings is deviated downward (because of the shape of the wngs) and, from the action-reaction law, the wings are pushed upward.

??? DUBBIO:

1. *discorso preso dal Crowe* : In the case of spherical particles, the fluid can be moved in a direction orthogonal to $\mathbf{u} - \mathbf{v}_p$ only in the presence of a rotation of the particle as a consequence of the no-slip condition on particle surface. Depending upon the fact that the particle rotation is caused by the presence of a gradient of fluid velocity or is imposed by external agents, the lift term is called respectively *Saffman* force or *Magnus* force.
2. *discorso preso da Michaelides(2003)i* (vedi [**?**] - par. *9a*) In the case of spherical particles, the fluid can be moved in a direction orthogonal to $\mathbf{u} - \mathbf{v}_p$ as a consequence of an asymmetry of the fluid streamlines around the particle; this asymmetry can be caused both by the presence of a gradient of fluid velocity (in this case the lift term is called *Saffman* force) or by a rotation of the particle (*Magnus* force).

Saffman force

The Saffman term is due to the presence of both a relative velocity $\mathbf{u} - \mathbf{v}_p$ between the *undisturbed ???* fluid and particle and a gradient of the *undisturbed ???* fluid velocity $\nabla \times \mathbf{u}$. A new particle Reynolds number (different from Re_p based on the relative velocity defined in equation 2.9) can be defined:

$$Re_G = \frac{d_p^2 \ |\nabla \times \mathbf{u}|}{\nu} \tag{2.29}$$

Saffman [**?**, **?**, **?**] considered the case $Re_p << Re_G^{0.5} << 1$
??? formula del Crowe

$$\mathbf{F}_{Saff} = 1.61 \ d_p^2 \ (\mu \ \rho)^{-0.5} \ [(\mathbf{u} - \mathbf{v}_p) \times (\nabla \times \mathbf{u})] \tag{2.30}$$

McLaughlin extended the study to the cases with $\epsilon = \frac{Re_G^{0.5}}{Re_p} < 1$
??? IL SIMBOLO ϵ L'HO RIPRESO DALLA MIA TESI ???
??? formule dal Crowe per il fattore correttivo (presa da Mei(1992)):

$$\frac{F_L}{F_{Saff}} = (1 - 0.3314\ \beta^{0.5})\ e^{-\left(\frac{Re_p}{10}\right)} + 0.3314\ \beta^{0.5} \qquad Re_p \leq 40 \quad (2.31)$$

$$= 0.0524\ (\beta\ Re_p)^{0.5} \qquad Re_p > 40 \quad (2.32)$$

where $\beta = \frac{d_p|\nabla\times\mathbf{u}|}{2\ |\mathbf{u}\times\mathbf{v}_p|} = \left(\frac{1}{2}\frac{Re_G}{Re_p}\right)$, $0.005 < \beta < 0.4$
??? METTERE UN GRAFICO E CONFRONTARE COL FATTORE CORRETIVO ϵ CHE HO USATO NELLA MIA TESI ???

Magnus force

??? formule copiate dal Crowe:
formula di Rubinow-Keller(1961)

$$\mathbf{F}_{Magn} = \frac{\pi}{8}\ d_p^2\ \rho \left[\left(\frac{1}{2}\nabla\times\mathbf{u} - \omega_p\right)\times(\mathbf{u}\times\mathbf{v}_p)\right] \quad (2.33)$$

where $\frac{1}{2}\nabla\times\mathbf{u}$ is the local fluid rotation and ω_p is the particle rotation velocity.
??????? ARRIVATO QUI ???????????????????????????? ??? nel Crowe (pag.95) dice che lift forces (sia Saffmann, sia Magnus) sono dovute a ROTAZIONE della particella
??? DISTINGUERE IN: - CASO GENERICO : TRIDIMENSIONALE - CASO DI LIFT RELATIVO AD UN GRADIENTE DI VELOCITA' PRINCIPALE (es.: grad. di vel. streamwise in direz. ortogonale alle pareti)

2.2.5 Added mass force

!!! is an *unsteady force* (i.e. related to the acceleration of the relative velocity) — see [**?**]
!!! it is also called *apparent mass* or *virtual mass*
def.: $\mathbf{F_{addm}}$ = forza richiesta per accelerare il fluido quando ho una variaz. della vel.relativa
!!! considera solo effetti inerziali (calcoli per ricavare la forza nel caso della sfera sono fatti con l'ipotesi di flusso ideale (inviscido e incomprimibile))

$$\mathbf{F_{addm}} = \frac{\rho\mathbf{V_p}}{\mathbf{2}}\left(\frac{\mathbf{Du}}{\mathbf{Dt}} - \frac{\mathbf{dv_p}}{\mathbf{dt}}\right) \quad (2.34)$$

where $\frac{D\mathbf{u}}{Dt}$ is the *material derivative* of $\mathbf{u}$ (??? in the case of incompressible flow $\frac{D\mathbf{u}}{Dt} = \frac{\partial\mathbf{u}}{\partial t} + \mathbf{u}\cdot\nabla\mathbf{u} = \frac{\partial\mathbf{u}}{\partial\mathbf{t}}$)
Correcting coefficient, from experiments on a sphere in simple armonic motion (Odar, Hamilton, 1964): $C_{addm} = 2.1 - \frac{0.132}{0.12+A_C^2}$ where A_C^2 is the acceleration parameter defined as $A_C^2 = \frac{u_r}{D\frac{du_r}{dt}}$

2.2.6 Basset history force

!!! is an *unsteady force* (i.e. related to the acceleration of the relative velocity) — see [**?**]

!!! is an *augmentation of the drag term* — see [**?**]

$$\mathbf{F_{bass}} = \frac{\mathbf{3}}{\mathbf{2}}\mathbf{d_p^2}\left(\pi\rho\mu\right)^{\mathbf{0.5}}\int_{\mathbf{0}}^{\mathbf{t}}\frac{\frac{\mathbf{Du}}{\mathbf{Dt}}-\frac{\mathbf{dv_p}}{\mathbf{dt}}}{\left(\mathbf{t}-\mathbf{t'}\right)^{\mathbf{0.5}}}\mathbf{dt'} \tag{2.35}$$

!!! CASES IN WHICH BASSET E ADDED MASS FORCES ARE INSIGNIFICANT (vedi Crowe pag.86):
- calculations of Hjemfelt and Mockros, 1966: $\rho/\rho_p \sim 10^{-3}$ and $\left(\mu/(\rho\omega d_p^2)\right)^{0.5} > 6$ where ω is the frequency of the oscillating flow
- calculations of Voir and Michaelides, 1994: $\rho/\rho_p < 0.002$ and $\omega\ \tau_p < 0.5$

2.2.7 Other forces

??? - METTERE SOLO CITAZIONE, DESCRIZIONE e REFERENCES ???

Electrical force

Magnetic force

Thermophoretic force

2.3 Summary

2.4 Exercices

NOTES

- Mettere capitolo per descrivere proprietá fisiche di fluido e particelle (viscositá, densitá, ...) e le relative uniti misura
- Gestione del rimbalzo alle pareti ??? Va messo nel capitolo "Advanced Topics" ???
- Distinzione tra particelle solide e droplets ??? In [**?**] (microhydrodynamic) considera *no-slip conditions* su particelle solide e *slip conditions* su interfaccia gassosi o liquidi
- Mettere capitolo su modifiche (o metodi alternaivi ???) dell'integrazione lagrangiana delle particelle: * Langevin equation * Monte-Carlo methods

3

Numerical Methods for Particle Tracking

Cristian Marchioli

3.1 Introduction

When dealing with tracking of particles with constant mass, we are interested in solving for the following equation:

$$\frac{\partial \mathbf{v}_p(t)}{\partial t} = \frac{\mathbf{F}[\mathbf{v}_p(t)]}{m_i} \ , \quad \mathbf{v}_p(t_0) = \mathbf{v}_{p,0} \ . \tag{3.1}$$

In general terms, this equation can be regarded as a first order ODE subject to an initial condition:

$$\frac{\partial}{\partial t}[\Phi(t)] = f[\Phi(t)] \ , \quad \Phi(t_0) = \Phi_0 \ ; \tag{3.2}$$

where $\Phi(t)$ is a matrix or array representing a set of variables (*e.g.* the particle velocity components). Thus, particle tracking is an initial value (or Cauchy) problem: first, the solution Φ_1 of the ODE at time $t_1 = t_0 + \Delta t$ has to be found. Φ_1 then becomes the new initial condition for computing Φ_2 at time $t_2 = t_1 + \Delta t$ and so on.

To this object, ODEs are solved numerically by converting derivatives into discrete algebraic expressions. This discretization procedure leads to an algebraic equation, which is manipulated to generate an algorithm for the approximate solution of the ODE. The algorithm gives the approximate solution at the $(n+1)-th$ time step in terms of the known solution at the $n-th$ and earlier time steps.

In this chapter, we review the most common time-marching numerical methods for ODEs.

3.2 Explicit and Implicit Methods

Equation 3.2 can be solved analitically by integration:

$$\int_{\Phi_n}^{\Phi_{n+1}} \mathrm{d}\Phi = \int_{t_n}^{t_{n+1}} f(t, \Phi(t))\ \mathrm{d}t\ . \tag{3.3}$$

However, approximation is required to evaluate the integral on the r.h.s. The *explicit method* (or *Euler forward*) replaces the integral with the initial value of the integrand operator f:

$$\frac{\Phi_{n+1} - \Phi_n}{\Delta t} = f(t_n, \Phi_n)\ . \tag{3.4}$$

The *implicit method* (or *Euler backward*) replaces the integral with the final value of the integrand operator f:

$$\frac{\Phi_{n+1} - \Phi_n}{\Delta t} = f(t_{n+1}, \Phi_{n+1})\ . \tag{3.5}$$

Another common method is the *midpoint rule* (or *modified Euler*), which uses the midpoint of the integration time interval:

$$\frac{\Phi_{n+1} - \Phi_n}{\Delta t} = f(t_{n+1/2}, \Phi_{n+1/2}). \tag{3.6}$$

The schematic in figure 3.1 shows the different procedures used by Euler schemes to approximate the integral on the r.h.s of equation 3.3, in comparison with the case of linear interpolation.

Note that Euler methods are first-order: the order of accuracy of the scheme by which the integration of the equation of particle motion is accomplished and the temporal resolution determine the magnitude of the error incurred at each time step. This error is accumulated over time and the cumulative time-stepping error depends also on the duration of tracking. In the case of Euler methods, the solution at the new time-step is computed with an error proportional to Δt^2, where Δt is the time step size. If N time steps are required to compute the solution at some finite final time $t = t_0 + N \cdot \Delta t$, then the final error is proportional to Δt.

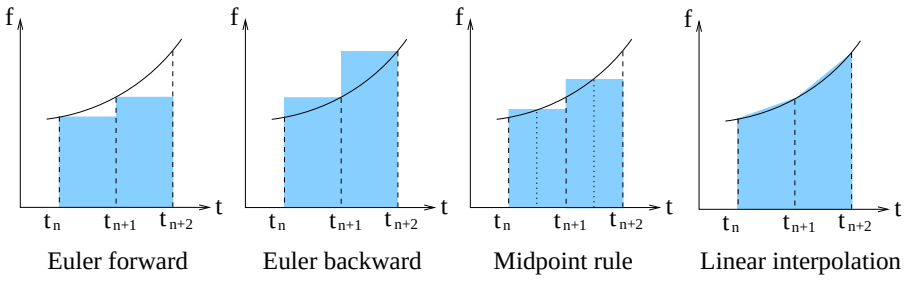

Fig. 3.1. Different procedure for the approximation of the time integral of $f(t, \Phi(t))$ over a finite time interval.

All methods thus produce accurate solutions when the time step size is small. However, many problems in fluid mechanics can only be solved by systems of differential equations that involve a wide range of different time scales. Such problems are said to be *stiff* in a certain interval of integration if the numerical solution in that interval has its step size limited more severely by the stability of the numerical technique than by the accuracy of the technique.

The issue of stability is briefly addressed in Appendix A of this book. The reader is referred to the books by Fletcher and by Ferziger and Peric for further details.

Here, it is important to underline that order of a scheme and stability are two different concepts. For example, the implicit schemes described above are unconditionally stable *i.e.* they yield bounded solutions for every time step if $\partial f(t,\Phi)/\partial\Phi < 0$ but their accuracy can be very limited.

Likewise, order of a scheme and accuracy of a scheme (*i.e.* the truncation error associated with approximating derivatives) are not the same thing. The order of a scheme is generally (tough not always) a reliable guide to the accuracy of that scheme. However, each scheme has its pathological applications which can cause it to break down. The order should be simply regarded as a quantitative measure of the rate at which the error decreases as the time step size decreases. In addition, this is true only when the time step size becomes smaller than a given threshold value, which depends on both the problem to be solved and the scheme used and can not be determined in advance. For time step size larger than the threshold value, the error yielded by two different schemes of the same order may differ by as much as an order of magnitude.

There is of course another requirement for accurate stable integration of the equations of motion. No particle can be allowed to move more than one grid cell in distance during each time step. In other words, the size of the tracking time step must be such that the typical displacement of a particle in any direction is smaller than the grid spacing in the same direction.

3.3 Predictor-Corrector Methods

Explicit Euler methods are generally more easy to program than implicit Euler methods. They also require less computer memory and CPU time per integration step, but they are more unstable. The idea behind *Predictor-Corrector Methods* (PCMs) is to combine the properties of explicit and implicit Euler methods to obtain a method with improved convergence characteristics. The most common PCM predicts the solution at the new time step using the explicit Euler method:

$$\Phi^*_{n+1} = \Phi_n + f(t_n, \Phi_n)\Delta t \ . \tag{3.7}$$

The predicted solution Φ^*_{n+1} is then corrected using the implicit trapezoidal rule (*i.e.* linear interpolation between the initial and the final points):

$$\Phi_{n+1} = \Phi_n + \frac{\Delta t}{2}\left[f(t_n, \Phi_n) + f(t_{n+1}, \Phi^*_{n+1}\right] \ . \tag{3.8}$$

It can be shown that the highest order of accuracy of such PCM is second-order. For higher orders, a suitable combination of Adams methods can be used (see Section 3.6).

3.4 Crank-Nicolson Methods

Crank-Nicolson Methods (CNMs) are implicit methods which apply the second-order trapezoidal rule to PDEs and ODEs:

$$\Phi_{n+1} = \Phi_n + \frac{\Delta t}{2}\left[f(t_n, \Phi_n) + f(t_{n+1}, \Phi_{n+1}\right] \ . \tag{3.9}$$

CNMs are commonly used when time accuracy is important. CNMs, Euler methods and PCMs are called two-level methods, since they involve the value of the unknown integral operator at only two time steps. The highest order of accuracy of two-level methods is second order. Higher-order approximations can be obtained by using methods which exploit the information at additional points. In the following, we discuss multi-step methods, which use previously generated solutions and Runge-Kutta methods, which use data at times between t_n and t_{n+1}.

3.5 Runge-Kutta Methods

As mentioned, multi-step methods achieve high order accuracy by efficiently using previously generated solutions. *Runge-Kutta Methods* (RKMs) achieve the same goal in a single step, but at the expense of many evaluations of the derivative per step. Being single-step schemes, RKM are self-starting and thus overcome the difficulties of starting multipoint methods using the specified initial condition. Also, they are more accurate and more stable than multipoint methods of the same order: thus, RKM work well with non-stationary process like particle dispersion studied in a Lagrangian framework.

The general n-step RK scheme applied to equation 3.3 can be written as:

$$\Phi_{n+1} = \Phi_n + \Delta t \sum_{r=1}^{R} c_r f^r \ , \tag{3.10}$$

where:

$$f^r = f(t_n + a_r \Delta t, \Phi_n + \Delta t \sum_{s=1}^{R} b_{rs} f^s) \ , \qquad a_r = \sum_{s=1}^{R} b_{rs} \ . \tag{3.11}$$

Note that b_{rs} are elements of a lower triangular matrix.

RKMs are classified as explicit, implicit and semi-implicit. Here, only the first two will be considered. Implicit schemes guarantee high accuracy and good stability but they are computationally expensive for non-linear initial value problems since they require the iterative solution of a set of non linear algebraic equations for f at each time step. This is much more expensive compared to the explicit schemes, which are easy to program and use less computer memory and computation time per step. Explicit methods, however, suffer from numerical instability when the time step is relatively large. The choice is a trade-off between stability and computational cost, if the schemes have the same order of accuracy. In general, implicit schemes are suitable for stiff differential equations whereas explicit RK schemes are more commonly used when the time step is small.

3.5.1 Second-order Runge-Kutta

The second-order RKM consists of two steps: the first step uses a first-order explicit Euler method to compute $\Phi^*_{n+1/2}$ at half time step, the second step uses the midpoint rule for the full time step to compute Φ_{n+1} at step $t_{n+1} = t_n + \Delta t$:

$$\Phi^*_{n+1/2} = \Phi_n + \frac{\Delta t}{2} f(t_n, \Phi_n) \ , \tag{3.12}$$

$$\Phi_{n+1} = \Phi_n + \Delta t f(t_{n+1/2}, \Phi^*_{n+1/2}) \ . \tag{3.13}$$

3.5.2 Third-order Runge-Kutta

The third-order RKM is derived using a higher order numerical integration scheme and consists of three steps. The first step uses a first-order explicit Euler method to compute $\Phi^*_{n+1/2}$; the second step uses the midpoint rule for the full time step to compute Φ^*_{n+1}. The final step uses the Simpson's rule to correct Φ^*_{n+1} and compute Φ_{n+1}.

$$\Phi^*_{n+1/2} = \Phi_n + \frac{\Delta t}{2} f(t_n, \Phi_n) \ , \tag{3.14}$$

$$\Phi^*_{n+1} = \Phi_n + \Delta t f(t_{n+1/2}, \Phi^*_{n+1/2}) \ , \tag{3.15}$$

$$\Phi_{n+1} = \Phi_n + \frac{\Delta t}{6} \left[f(t_n, \Phi_n) + 4 f(t_{n+1}, \Phi^*_{n+1}) + \right. \tag{3.16}$$

$$\left. f(t_{n+1}, \Phi^{**}_{n+1}) \right] \ . \tag{3.17}$$

where $\Phi^{**}_{n+1} = \Phi_n + 2(\Phi^*_{n+1} - \Phi^*_{n+1/2})$. A second version is obtained by splitting the integration time step in three parts, as shown in figure 3.2:

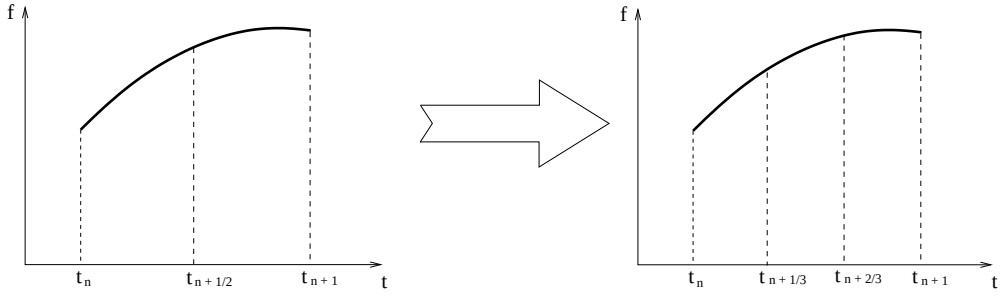

Fig. 3.2. Time step splitting: a) 2nd-order RKM, b) 3rd-order RKM.

$$\Phi^*_{n+1/3} = \Phi_n + \frac{\Delta t}{3} f(t_n, \Phi_n) \ , \tag{3.18}$$

$$\Phi^*_{n+2/3} = \Phi_n + \frac{2\Delta t}{3} f(t_{n+1/3}, \Phi^*_{n+1/3}) \ , \tag{3.19}$$

$$\Phi_{n+1} = \Phi_n + \frac{\Delta t}{4} \left[f(t_n, \Phi_n) + 3 f(t_{n+2/3}, \Phi^*_{n+2/3}) \right] \ . \tag{3.20}$$

3.5.3 Fourth-order Runge-Kutta

The fourth-order RKM is the most popular among higher-order RKMs and consists of four steps. The first two steps use a first-order explicit Euler predictor and a first-order implicit Euler corrector to compute $\Phi^*_{n+1/2}$ and $\Phi^{**}_{n+1/2}$ at half time step. The third step uses the midpoint rule for the full time step to predict Φ^*_{n+1} which is corrected in the final step by means of the Simpson's 1/3 rule.

$$\Phi^*_{n+1/2} = \Phi_n + \frac{\Delta t}{2} f(t_n, \Phi_n) \ , \tag{3.21}$$

$$\Phi^{**}_{n+1/2} = \Phi_n + \frac{\Delta t}{2} f(t_{n+1/2}, \Phi_{n+1/2}) \ , \tag{3.22}$$

$$\Phi^*_{n+1} = \Phi_n + \Delta t f(t_{n+1/2}, \Phi^{**}_{n+1/2}) \ , \tag{3.23}$$

$$\Phi_{n+1} = \Phi_n + \frac{\Delta t}{6} \left[f(t_n, \Phi_n) + 2 f(t_{n+1/2}, \Phi^*_{n+1/2}) + 2 f(t_{n+1/2}, \Phi^{**}_{n+1/2}) + f(t_{n+1}, \Phi^*_{n+1}) \right] \ . \tag{3.24}$$

A second (less popular) version is based on the Simpson's 3/8 rule and reads:

$$\Phi^*_{n+1/3} = \Phi_n + \frac{\Delta t}{3} f(t_n, \Phi_n) \ , \tag{3.25}$$

$$\Phi^*_{n+2/3} = \Phi_n + \frac{2\Delta t}{3} f(t_{n+1/3}, \Phi^*_{n+1/3}) \ , \tag{3.26}$$

$$\Phi^{**}_{n+2/3} = \Phi^*_{n+2/3} + \frac{\Delta t}{3}\left[f(t_{n+1/3}, \Phi^*_{n+1/3}) - f(t_n, \Phi_n)\right] \ , \tag{3.27}$$

$$\Phi^*_{n+1} = \Phi_n + \Delta t\left[f(t_n, \Phi_n) - f(t_{n+1/3}, \Phi^*_{n+1/3}) + f(t_{n+2/3}, \Phi^{**}_{n+2/3})\right] \ , \tag{3.28}$$

$$\Phi_{n+1} = \Phi_n + \frac{\Delta t}{8}\left[f(t_n, \Phi_n) + 3f(t_{n+1/3}, \Phi^*_{n+1/3}) + 3f(t_{n+2/3}, \Phi^{**}_{n+2/3}) + f(t_{n+1}, \Phi^*_{n+1})\right] \ . \tag{3.29}$$

3.6 Adams Methods

Adams methods are multipoint methods derived by fitting a polynomial to the derivatives at a number of points in time. Explicit Adams methods use data at time t_n in the interpolation polynomial and are known as *Adams-Bashforth Methods* (ABMs). Implicit Adams methods use data at time t_{n+1} and are known as *Adams-Moulton Methods* (AMMs). The first-order explicit/implicit Adams Method is explicit/implicit Euler.

Second-order Adams-Bashforth Method:

$$\Phi_{n+1} = \Phi_n + \frac{\Delta t}{2}\left[3f(t_n, \Phi_n) - f(t_{n-1}, \Phi_{n-1})\right] \ . \tag{3.30}$$

Second-order Adams-Moulton Method:

$$\Phi_{n+1} = \Phi_n + \frac{\Delta t}{2}\left[f(t_n, \Phi_n) + f(t_{n+1}, \Phi_{n+1})\right] \ . \tag{3.31}$$

The second-order AMM is the same as the second-order CNM: thus, it does not use previously computed solution values. The third order formula is more typical because it does involve a previously computed value. For completeness, third-order and fourth-order ABM and AMM are reported (for sake of brevity, we put $f(t, \Phi) = f$).

Third-order and forth-order ABM:

$$(3^{rd}\text{-order}) \ \Phi_{n+1} = \Phi_n + \frac{\Delta t}{12}\left(23f_n - 16f_{n-1} + 5f_{n-2}\right) \ , \tag{3.32}$$

$$(4^{th}\text{-order}) \ \Phi_{n+1} = \Phi_n + \frac{\Delta t}{24}\left(55f_n - 59f_{n-1} + 37f_{n-2} - 9f_{n-3}\right) \ . \tag{3.33}$$

Third-order and forth-order AMM:

$$(3^{rd}\text{-order})\ \Phi_{n+1} = \Phi_n + \frac{\Delta t}{12}\left(5f_{n+1} + 8f_n - f_{n-1}\right)\ , \quad (3.34)$$

$$(4^{th}\text{-order})\ \Phi_{n+1} = \Phi_n + \frac{\Delta t}{24}\left(9f_{n+1} + 19f_n - 5f_{n-1} + f_{n-2}\right)\ . \quad (3.35)$$

Adams methods of order higher than four exist but they are not often used for the solution of ODEs. Interestingly, Adams methods can be combined to obtain PCMs of order higher than second: a common procedure is to use a 3rd/4th order ABM as a predictor and a AMM of the same order as a corrector.

The Adams-Moulton formula is more accurate than the Adams-Bashforth formula of the same order, so that it can use a larger step size; the Adams-Moulton formula is also more stable. A modern code based on Adams methods is relatively easy to program and requires only one evaluation of the derivative per time step. However, it may produce non-physical solutions due to the use of data from several time steps. Another drawback is that an Adams code is more complex than a Runge-Kutta code because it must cope with the difficulties of starting the integration and adapting the time step size. With enough "memorized" values, however, we can use whatever order formula we wish in the step from t_0. Modern Adams codes attempt to select the most efficient formula at each step as well as to choose an optimal step size to achieve a user-specified accuracy.

Some general rules-of-thumb about how to choose between Runge-Kutta methods and Adams methods are given below:

1. If output at many points is needed, Adams methods are generally preferred.
2. If function evaluations are expensive, Adams methods are preferred.
3. If function evaluations are inexpensive and moderate accuracy is required, Runge-Kutta methods are generally best.
4. If storage is at a premium, Runge-Kutta methods are preferred.
5. If accuracy over a wide range of tolerances is needed, the variable order Adams methods will outperform the fixed order Runge-Kutta methods.

3.7 Integration Time Step Size Considerations

The choice of the time step size is crucial in particle tracking: it must be chosen correctly to perform the numerical experiments and to compute the Lagrangian statistics efficiently and accurately.

A theorem, developed by H. Nyquist, states that a signal may be uniquely reconstructed, without error, from samples taken at equal time intervals. The sampling rate (the number of samples taken per unit time, *i.e.* the rate at which the signal is sampled for subsequent use) must be equal to, or greater than, twice the highest frequency component in the signal. If we apply Nyquist's theorem to particle tracking, the tracking time step, Δt_{Tr}, is

the "highest frequency component" and the particle response time τ_p is the "sampling rate" so that it must be:

$$\Delta t_{Tr} \leq \frac{\tau_p}{2} \ , \tag{3.36}$$

in order to obtain an accurate estimate of the particle trajectory, which is the "signal" to be reconstructed.

The magnitude of the time step Δt_{Tr} is bounded not only by the resolution required to compute accurate particle trajectories but also by the available computer disk space. A smaller Δt_{Tr} requires higher storage frequency and larger disk space. On the other hand, accurate particle trajectories need Δt_{Tr} to be smaller than particle characteristic time τ_p. As a consequence, the three-dimensional fluid velocity field needs to be stored at intervals equal to Δt_{Tr}, which is larger than the time step, Δt_{NS}, used in integrating the Navier-Stokes equations for the fluid. A common procedure is to choose $\Delta t_{Tr} = \Delta t_{NS}$ (van Harleem *et al.* 1998).

In their DNS of particle dispersion in a decaying isotropic turbulence, Elghobashi & Truesdell (1992) used $\Delta t_{Tr} = (1/2 \div 1/3)\ \tau_p$ on a 96^3 points grid: the disk space required to store the three fluid velocity components was 10 Mb per time step. Roughly 1 Gb of disk space was required for the complete trajectory of each of the 22^3 tracked particles. A further reduction of the time step size ($\Delta t_{Tr} = 1/4\ \tau_p$) resulted in a negligible difference in the dispersion statistics.

Further comments can be done considering the dependency of the time step size on the character of the turbulence, most likely the integral time scale, the particle's inertia and the particle's settling velocity. Intuitively, we know that, as the Stokes number increases, particles tend not to respond to the acceleration of the surrounding fluid and follow a trajectory quite different than that of the fluid particles. Also, particles with small settling velocity show no preferred direction whereas particles with large settling velocity tend to drift in the direction of the external body force acting on them. In both situations, it is not straightforward to guess which case requires the smallest time step to keep the overall error low (Wang & Stock, 1992).

Results reported in the literature show that:

- the error in the particle location relative to an exact trajectory grows exponentially with time, no matter how small the time step (Wang & Stock, 1992). The smaller the time step size, the longer it takes for the error to become significant.
- if the long-time particle diffusivity is to be calculated, the error in the particle location should be low after several Lagrangian integration times. To this aim, a smaller time step is required with increasing particle Stokes number, St, and settling velocity, $\mathbf{v}_s$. The decrease in the time step size with increasing St (*i.e.* increasing particle mass) is mostly due to the increase in the Lagrangian integration time. The decrease in the time step

size with increasing $\mathbf{v}_s$ is due to the increase in the distance traveled by the particle.

- if the behavior of particle trajectories at a given time after release is of interest, then the time step size limit should be determined for a fixed total Lagrangian integration time. To this aim, larger time steps can be used for particles with larger inertia (*i.e.* larger St), because the trajectories are less random.

The time required to accomplish a simulation for heavy particle dispersion depends on the total Lagrangian integration time, the time step size, the number of particle trajectories computed [1]. In the dispersion simulation by Wang & Stock (1992), 2000 particle trajectories were calculated using 80 Fourier modes: the computation time on a IBM 3090 computer ranged from 2500 to 8000 seconds.

3.8 Application to the Generic Particle Equation of Motion

We next consider the application of some of the numerical schemes described in the previous paragraphs to the equation of motion for a spherical particle subject to drag force only, in the hypotesis of Stokes regime:

$$\frac{\mathrm{d}v_p}{\mathrm{d}t} = \frac{u - v_p}{\tau_p} \tag{3.37}$$

We discretize equation 3.37 and write down the expressions for its solution $v_{p,n+1}$ at the new time step t_{n+1}.

1. Euler explicit:

$$v_{p,n+1} = v_{p,n} + \frac{\Delta t}{\tau_p}\left(u_n - v_{p,n}\right)$$

2. Euler implicit:

$$v_{p,n+1} = v_{p,n} + \frac{\Delta t}{\tau_p}\left(u_{n+1} - v_{p,n+1}\right) \rightarrow v_{p,n+1} = \frac{v_{p,n} + \frac{\Delta t}{\tau_p} u_{n+1}}{1 + \frac{\Delta t}{\tau_p}}$$

3. Predictor-corrector:

$$v^*_{p,n+1} = v_{p,n} + \frac{\Delta t}{\tau_p}\left(u_n - v_{p,n}\right)$$

$$v_{p,n+1} = v_{p,n} + \frac{\Delta t}{2\tau_p}\left[\left(u_n - v_{p,n}\right) + \left(u_{n+1} - v^*_{p,n+1}\right)\right]$$

[1] and the number of Fourier modes to simulate the fluid, if a pseudo-spectral DNS code is used.

4. 2nd-order RK:

$$v^*_{p,n+1/2} = v_{p,n} + \frac{\Delta t}{2\tau_p}\left(u_n - v_{p,n}\right)$$

$$v_{p,n+1} = v_{p,n} + \frac{\Delta t}{\tau_p}\left(u_{n+1/2} - v^*_{p,n+1/2}\right)$$

5. 3rd-order RK:

$$v^*_{p,n+1/2} = v_{p,n} + \frac{\Delta t}{2\tau_p}\left(u_n - v_{p,n}\right)$$

$$v^*_{p,n+1} = v_{p,n} + \frac{\Delta t}{\tau_p}\left(u_{n+1/2} - v^*_{p,n+1/2}\right)$$

$$v_{p,n+1} = v_{p,n} + \frac{\Delta t}{6\tau_p}\left[(u_n - v_{p,n}) + 4(u_{n+1/2} - v^*_{p,n+1/2}) + (u_{n+1} - v^*_{p,n+1})\right]$$

6. 4th-order RK:

$$v^*_{p,n+1/2} = v_{p,n} + \frac{\Delta t}{2\tau_p}\left(u_n - v_{p,n}\right)$$

$$v^{**}_{p,n+1/2} = v_{p,n} + \frac{\Delta t}{2\tau_p}\left(u_{n+1/2} - v^*_{p,n+1/2}\right)$$

$$v^*_{p,n+1} = v_{p,n} + \frac{\Delta t}{\tau_p}\left(u_{n+1/2} - v^{**}_{p,n+1/2}\right)$$

$$v_{p,n+1} = v_{p,n} + \frac{\Delta t}{6\tau_p}\left[(u_n - v_{p,n}) + 2(u_{n+1/2} - v^*_{p,n+1/2}) + \right.$$
$$\left. + 2(u_{n+1/2} - v^{**}_{p,n+1/2}) + (u_{n+1} - v^*_{p,n+1})\right]$$

7. 2nd-order AM (and 2nd-order CN):

$$v_{p,n+1} = v_{p,n} + \frac{\Delta t}{2\tau_p}\left[(u_n - v_{p,n}) + (u_{n+1} - v_{p,n+1})\right]$$
$$\rightarrow v_{p,n+1} = \frac{v_{p,n} + \frac{\Delta t}{2\tau_p}(u_{n+1} + u_n - v_{p,n})}{1 + \frac{\Delta t}{2\tau_p}}$$

8. 2nd-order AB:

$$v_{p,n+1} = v_{p,n} + \frac{\Delta t}{2\tau_p}\left[3(u_n - v_{p,n}) - (u_{n-1} - v_{p,n-1})\right]$$

9. 3rd-order AM:

$$v_{p,n+1} = v_{p,n} + \frac{\Delta t}{12\tau_p}\left[5(u_{n+1} - v_{p,n+1}) + 8(u_n - v_{p,n}) - (u_{n-1} - v_{p,n-1})\right]$$
$$\rightarrow v_{p,n+1} = \frac{v_{p,n} + \frac{\Delta t}{12\tau_p}\left[5u_{n+1} + 8(u_n - v_{p,n}) - (u_{n-1} - v_{p,n-1})\right]}{1 + \frac{5\Delta t}{12\tau_p}}$$

10. 3rd-order AB:

$$v_{p,n+1} = v_{p,n} + \frac{\Delta t}{12\tau_p}\left[23(u_n - v_{p,n}) - 16(u_{n-1} - v_{p,n-1}) + 5(u_{n-2} - v_{p,n-2})\right]$$

11. 4th-order AM:

$$v_{p,n+1} = v_{p,n} + \frac{\Delta t}{24\tau_p}\left[9(u_{n+1} - v_{p,n+1}) + 19(u_n - v_{p,n})\right.$$
$$\left.-5(u_{n-1} - v_{p,n-1}) + (u_{n-2} - v_{p,n-2})\right]$$

12. 4th-order AB:

$$v_{p,n+1} = v_{p,n} + \frac{\Delta t}{24\tau_p}\left[55(u_n - v_{p,n}) - 59(u_{n-1} - v_{p,n-1})\right.$$
$$\left.+37(u_{n-2} - v_{p,n-2}) - 9(u_{n-3} - v_{p,n-3})\right]$$

Note that the fluid velocities interpolated at particle position at time $t_{n+1/2}$ and/or t_{n+1}, namely $u_{n+1/2}$ and u_{n+1}, may be required to calculate $v_{p,n+1}$. These velocities are unknown *a priori* and have to be estimated: thus, some approximation is necessary. The easiest (and less accurate) choice is to freeze the fluid velocity field during the time interval between t_n and t_{n+1}, so that $u_n = u_{n+1/2} = u_{n+1}$. This approximation is justified as follows: the time step size Δt_{NS} used in the solution of the Navier-Stokes equation for the fluid is limited by the Courant numerical stability constraint and is typically much smaller than the time step size Δt_{Tr} used in the integration of the particle equation of motion (Kontomaris, Hanratty & McLaughlin 1992). In fact, Δt_{NS} is much smaller than the Kolmogorov fluid time-scale fluctuations based on the volume-averaged viscous dissipation. Another option is to interpolate $u_{n+1/2}$ at particle position at time $t_{n+1/2}$ and u_{n+1} at particle position at time t_{n+1}. To this aim, the particle velocity $v^*_{p,n+1/2}$ and $v^*_{p,n+1}$ predicted by the numerical method can be used.

In order to demonstrate the performance of the different numerical schemes, in figure 3.3, we compare the behavior of the solution of equation 3.37 when Euler methods, PCMs amd Adams methods are used.

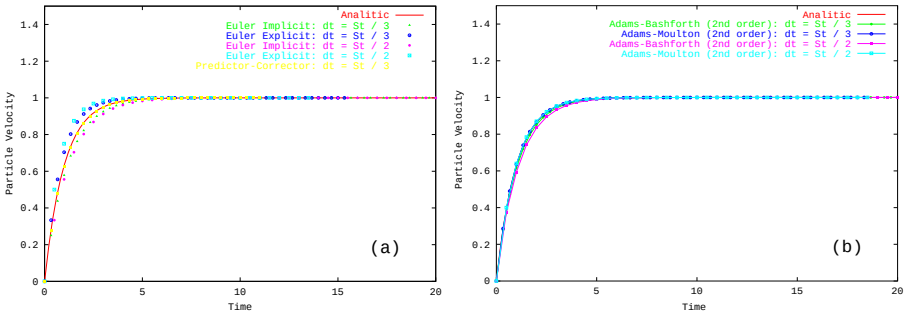

Fig. 3.3. Behavior of the solution by explicit/implicit Euler methods and by second-order PCM (a) and by second-order ABM/AMM (b) using two different time step sizes: $\Delta t = St/2$ and $\Delta t = St/3$.

From figure 3.3a, it is apparent that second-order PCMs produce a more accurate solution than first-order Euler methods. As expected, the implicit Euler method tends to slighlty underpredict whereas the explicit Euler method tends to overpredict the correct value of the solution. Also, the accuracy of Euler methods significantly increases as the time step size decreases. From figure 3.3b, it is apparent that AMMs are more accurate than ABMs of the same order and that the accuracy of both methods increases as the time step size decreases.

Figure 3.4 shows what happens when a numerical scheme is used with time steps which violate the stability condition. We used a fourth-order explicit ABM (figure 3.4a): when the time step size is equal to half the particle Stokes number ($\Delta t = St/2$), oscillations are generated which grow unboundedly with time. In a few steps, the numbers become too large to be handled by the computer. When the computation is carried on with a time step size $\Delta t = St/3$, oscillations are still generated but they grow much slower. Eventually, oscillations disappear with a further reduction of the time step size ($\Delta t = St/4$ and $\Delta t = St/5$ profiles). With an implicit AMM of the same order (figure 3.4b) no problems occurred even for the largest time step used.

Figure 3.5 shows what happens when the time step size is fixed and the order of the numerical scheme is changed. When an explicit ABM is used (figure 3.5a), increasing the order of the method triggers small amplitude oscillations which slowly grow with time. This problem does not occur with the implicit AMM counterpart (figure 3.5b).

Figure 3.6 shows the behavior of the solution when a RKM is used: both the order of the scheme and the time step size are increased. No oscillation in the solution occurs (recall that RMKs are more stable than Adams methods of the same order) but the accuracy significantly decreases as the time step size increases from $\Delta t = St/3$ (figure 3.6a) to $\Delta t = 1.5\ St$ (figure 3.6d). Of course, higher-order RKMs yield more accurate solution for a given time step size.

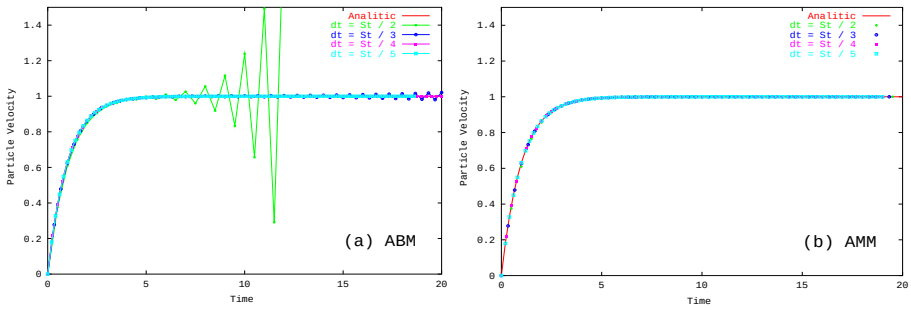

Fig. 3.4. Behavior of the solution by fourth-order ABM (a) and AMM (b) as the time step size Δt is reduced from $\Delta t = St/2$ to $\Delta t = St/5$.

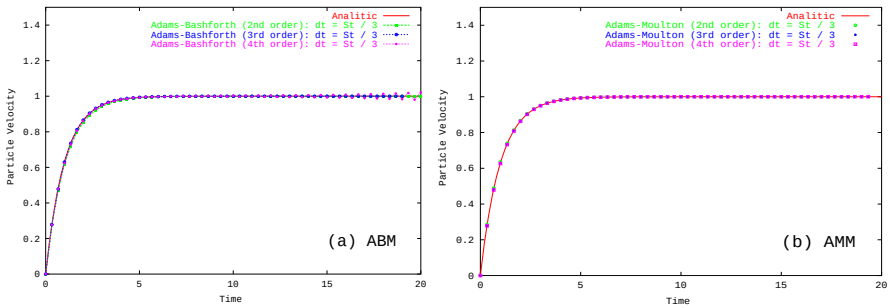

Fig. 3.5. Behavior of the solution by second-, third- and fourth-order ABM (a) and AMM (b) using a time step size $\Delta t = St/3$.

In figure 3.7 the temporal discretization error is shown for various time integration schemes. The discretization error is obtained by subtracting the numerical solution to the exact analytic solution of equation 3.37.

The two Euler methods show the expected first-order behavior: the error and the time step size both reduce by the same amount. The implicit Euler scheme is more accurate than the explicit Euler counterpart but the difference in the solution provided by the two schemes decreases as the time step size decreases.

The second-order schemes show also the expected error reduction rate. The second-order ABM (started by the second-order RKM) yields a larger initial error than both the PCM and the AMM (also started by the second-order RKM) of the same order but the error reduction rate remains the same. Recall that the second-order AMM is the same as the second-order CNM.

A slight difference in the accuracy of the solution occurs when Adams methods of the third-order are used: the ABM provides a slightly larger initial error than AMM but the error reduction rate is again the same as the time step size decreases. We do not show here the estimates of the temporal

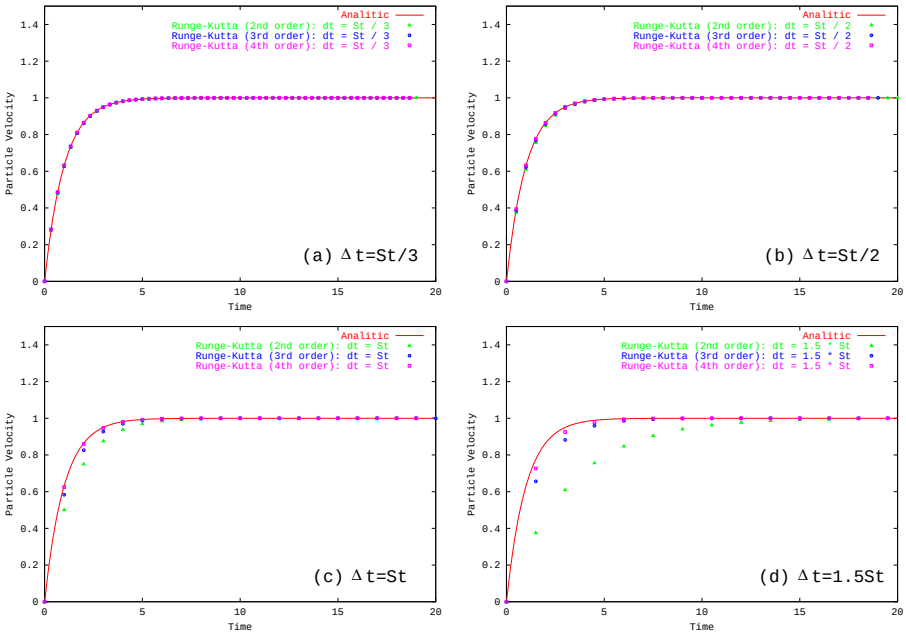

Fig. 3.6. Behavior of the solution by second, third and fourth-order RKM as the time step size Δt is increased from $\Delta t = St/3$ to $\Delta t = 1.5St$.

discretization error for the forth-order Adams methods, due to the oscillatory solution provided by the ABM (see figure 3.4).

The forth-order RKM is by far the most accurate scheme: the error is about four orders of magnitude smaller than that of Euler methods and it is reduced by two orders of magnitude over the time step size reduction considered.

To investigate further the accuracy of temporal discretization, in figure 3.8 we evaluate the convergence of particle velocity as the time step size is reduced. We compare the exact solution of equation 3.37 at time $t = 4.0$ with the numerical solution provided by the schemes already considered in figure 3.7. We performed calculations up to that time using 8, 12, 16 and 20 time steps corresponding to time step sizes of $\Delta t = St/2$, $\Delta t = St/3$, $\Delta t = St/4$, $\Delta t = St/5$ respectively. The convergence rate is consistent with the results shown in figure 3.7. The implicit Euler, the second-order PCM, RKM and ABM underpredict the exact value. The explicit Euler and the second-order AMM (*i.e.* CNM) overpredict the exact value. All schemes show monotonic convergence towards the exact time step independent solution. As expected, the most accurate reference solution is obtained using the forth-order RKM.

To conclude this chapter, we point out that the interpolation error, which mainly depends on the spatial resolution of the small-scale motions of the tubrulent flow (see Chapter 4), is always the major source of numerical errors in the extraction of Lagrangian data. The time-stepping error is generally

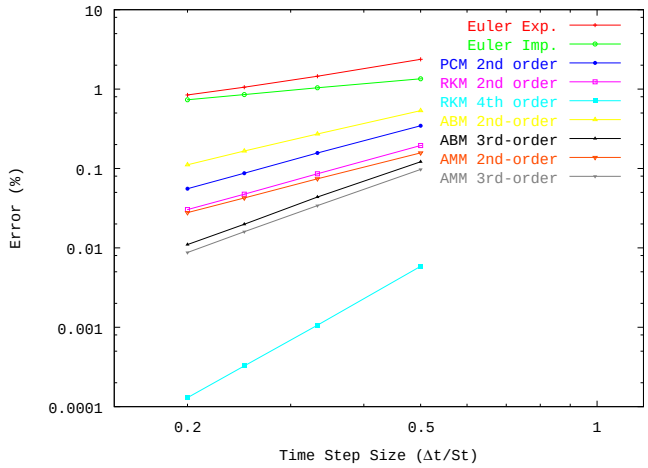

Fig. 3.7. Temporal discretization error for various time integration schemes.

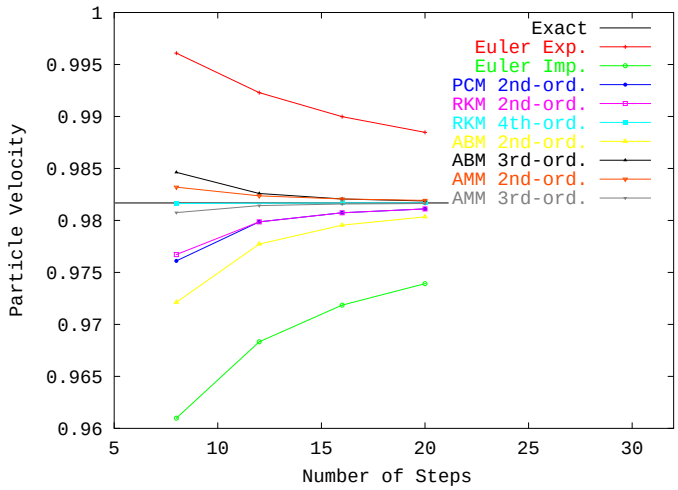

Fig. 3.8. Convergence of v_p at time $t = 4.0$ as the time step size is reduced for various time integration schemes.

less significant because it is restricted to small values by enforcement of the Courant number stability limit (Yeung and Pope, 1988; Yeung and Pope, 1989).

Appendix A

Consider the particle equation of motion in the following form:

$$\frac{\partial v_i^n}{\partial t} = \frac{F(x_i^n)}{m_i} , \qquad \frac{\partial x_i^n}{\partial t} = v_i^n , \tag{3.54}$$

where v_i^n is particle velocity at time t^n at its position x_i^n. The term $F(x_i^n)$ represents the external forces acting on the particle of mass m_i. Combining the above equations into one we get:

$$\frac{\partial^2 x_i^n}{\partial t^2} = \frac{F(x_i^n)}{m_i} , \tag{3.55}$$

where x_i^n is the numerical solution at time t^n. Now, let X_i^n be the exact solution of equation 3.55 at time t^n, that is the solution without round-off error [2]. The numerical error at time t^n can be defined as:

$$\epsilon_i^n = x_i^n - X_i^n . \tag{3.56}$$

Using equation 3.56 to replace x in equation 3.55, an equation for the time evolution of the error ϵ^n is obtained:

$$\frac{\partial^2 \epsilon_i^n}{\partial t^2} = \frac{F(X_i^n + \epsilon_i^n)}{m_i} - \frac{\partial^2 X_i^n}{\partial t^2} . \tag{3.57}$$

Observe that:

$$\frac{\partial^2 X_i^n}{\partial t^2} = \frac{F(X_i^n)}{m_i} , \tag{3.58}$$

and that:

$$F(X_i^n + \epsilon_i^n) - F(X_i^n) = \left.\frac{\partial F}{\partial X}\right|_{X_i^n} \cdot \epsilon_i^n , \tag{3.59}$$

in the limit $\epsilon_i^n \to 0$. Thus, equation 3.57 can be rewritten as:

$$\frac{\partial^2 \epsilon_i^n}{\partial t^2} = \frac{1}{m_i} \left.\frac{\partial F}{\partial X}\right|_{X_i^n} \cdot \epsilon_i^n . \tag{3.60}$$

Assume to approximate the l.h.s. of equation 3.60 by means of a simple central-difference three time-level scheme (also known as leapfrog method [3]):

[2] The round-off error is the error introduced because the computer only stores numbers up to a certain precision.

[3] The leapfrog method is the application of the midpoint rule to an integration interval of size $2\Delta t$

$$\frac{\epsilon_i^{n+1} - 2\epsilon_i^n + \epsilon_i^{n+1}}{\Delta t^2} = \frac{1}{m_i} \left.\frac{\partial F}{\partial X}\right|_{X_i^n} \cdot \epsilon_i^n \ . \tag{3.61}$$

For bounded oscillatory solutions of the form:

$$\epsilon_i^n = (\lambda)^n = (e^{i\omega\Delta t})^n \ , \tag{3.62}$$

equation 3.60 can be recast as:

$$\lambda^2 - \lambda \cdot \left(2 + \frac{\Delta t^2}{m_i} \left.\frac{\partial F}{\partial X}\right|_{X_i^n} \right) + 1 = 0 \tag{3.63}$$

Assuming $\frac{\Delta t^2}{m_i} \cdot \left.\frac{\partial F}{\partial X}\right|_{X_i^n} = \beta$, this equation has two solutions:

$$\lambda_{1,2} = 1 + \frac{\beta}{2} \cdot \left(1 \pm \sqrt{1 + \frac{4}{\beta}} \right) \ , \tag{3.64}$$

which correspond to the error amplification factor. The general solution is:

$$\epsilon_i^n = C_1 \cdot \lambda_1 + C_2 \cdot \lambda_2 \ . \tag{3.65}$$

The scheme is said to be *conditionally stable* provided $|\lambda_{1,2}| \leq 1$. Figure 3.9 shows the behavior of λ_1 and λ_2 as a function of $i\sqrt{\beta}$. When $i\sqrt{\beta} < 2$, λ_1 and λ_2 have an imaginary part, but for $i\sqrt{\beta} \geq 2$ both solutions are real. Complex values must be considered because higher order systems may exhibit complex eigenvalues. Values with zero or negative real part must be considered because they lead to bounded solutions.

For $i\sqrt{\beta} < 2$, it can be shown that $|\lambda_{1,2}| = 1$: not only is the leapfrog scheme stable but also it suffers no amplitude dissipation. When $i\sqrt{\beta} > 2$, $|\lambda_2| > 1$: to guarantee stability, we must calculate the largest value of $\mid m_i^{-1} \partial F / \partial X \mid$ and then set Δt such that:

$$\Delta t < \frac{2}{\sqrt{\left| \frac{1}{m_i} \frac{\partial F}{\partial X} \right|}} \ . \tag{3.66}$$

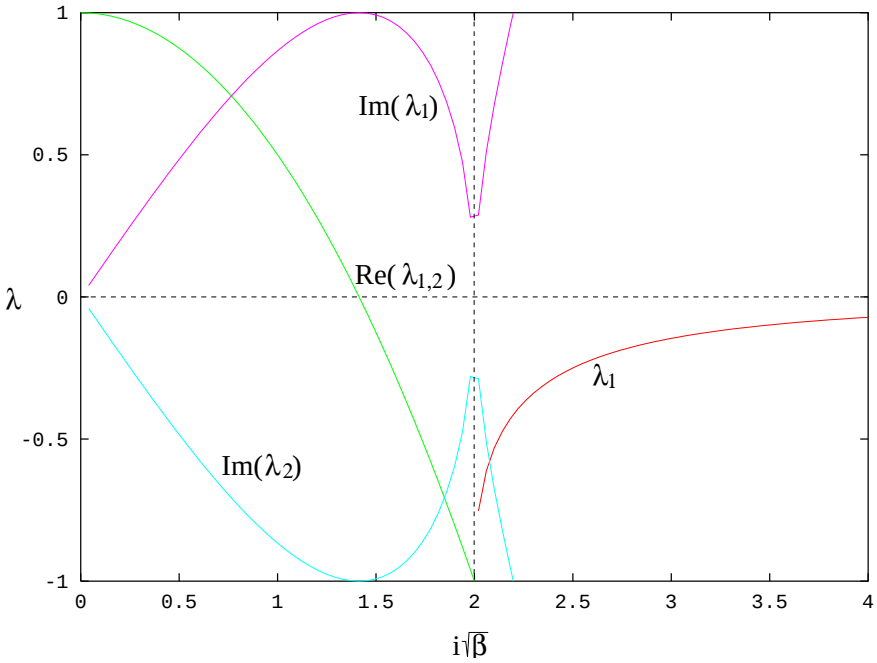

Fig. 3.9. The roots of equation 3.9 as a function of $i\sqrt{\beta}$. For $i\sqrt{\beta} < 2$ both roots have an imaginary component, but both have magnitude $|\lambda_{1,2}| < 1$. For $i\sqrt{\beta} < 2$ both roots are real and $|\lambda_2| < 1$.

3.9 Bibliography

1. Elghobashi, S. & Truesdell, G.C. (1992). Direct simulation of particle dispersion in a decaying isotropic turbulence. *J. Fluid Mech.*, **242**, 655-700.
2. Ferziger, J.H. & Peric, M. (1997). *Computational Methods for Fluid Dynamics.* Springer-Verlag.
3. Fletcher, C.A.J. (2000). *Computational Techniques for Fluid Dynamics.* Springer-Verlag.
4. van Haarlem, B., Boersma, B.J. & Nieuwstadt, T.M. (1998). Direct numerical simulation of particle deposition onto a free-slip and no-slip surface. *Phys. Fluids*, **10**, 2608-2620.
5. Kontomaris, K., Hanratty, T.J. & McLaughlin, J.B. (1992). An algorithm for tracking fluid particles in a spectral simulation of turbulent channel flow. *J. Comput. Phys.*, **103**, 231-242.
6. Wang, L.P. & Stock, D.E. (1992). Numerical simulation of heavy particle dispersion time step and nonlinear drag considerations. *J. Fluids Eng.*, **114**, 100-106.

7. Yeung, P.K. & Pope, S.B. (1988). An algorithm for tracking fluid particles in numerical simulation of homogeneous turbulence. *J. Comput. Phys.*, **79**, 373-416.
8. Yeung, P.K. & Pope, S.B. (1989). Lagrangian statistics from direct numerical simulations of isotropic turbulence. *J. Fluid Mech.*, **207**, 531-586.

4

Interpolation

4.1 Generalities

In studying particle motion with numerical flow simulations it is necessary to evaluate the local fluid velocity at particle position which, in general, does not coincide with a point of the mesh used for the flow field simulation. The numerical solution of the fluid velocity field is available only in correspondence of these grid points, which represent the discretization of the physical domain; so numerical interpolation must be used to evaluate the flow field velocity at particle position. Three approaches exist in order to discretize and solve numerically a physical problem: finite difference, finite volume and finite element methods (Ferziger and Peric 1996, Fletcher 2000). In all of the above methods the grid spacing between the grid-points, Δx [1], is a crucial parameter that determines the accuracy of the discretization methods. This parameter is very important since it determines the order of magnitude of the interpolation error (Yeung and Pope 1988).

Following Balachandar and Maxey (1989) in each of the interpolation methods the 3-dimensional fluid velocity $\mathbf{u}(x, y, z, t)$ is approximated by a series of the form:

$$\mathbf{v}(x, y, z, t) = \sum_{n} \sum_{m} \sum_{l} \mathbf{a}(n, m, l) f_n(x) g_m(y) h_l(z), \tag{4.1}$$

evaluated at the coordinate position (x, y, z). Functions $f_n(x)$, $g_m(y)$, $h_l(z)$ are the basis functions and $\mathbf{a}(n, m, l)$ are the coefficients. The choice of the basis functions and the coefficients depends on the velocity evaluation method.

[1] $\Delta x = x_i - x_{i-1}$ where x_i and x_{i-1} are two consecutive grid point coordinates.

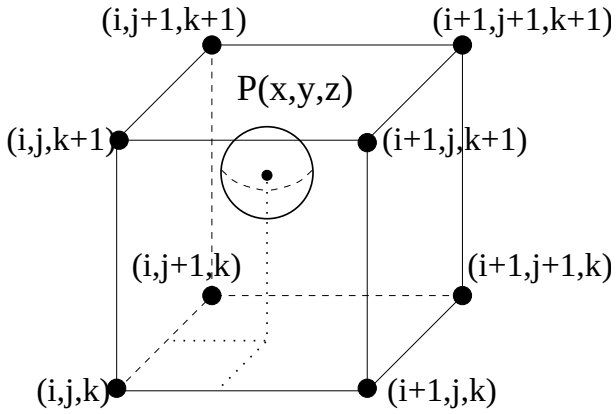

Fig. 4.1. Sketch of a particle P(x,y,z) in a cubic cell

4.2 Interpolation Schemes

There are several methods for evaluating the fluid velocity at particle position. We will describe the most common interpolation schemes applied in lagrangian particle tracking in regular grids.

4.2.1 Linear

Linear interpolation in three directions has been widely used because of its simplicity. This linear scheme involves only the nodal values at the 8 vertices of the interpolation cell (nodes to 1 to 8). It approximates the dependent variable within the cell as a linear function in each coordinate. Since such a function has 8 coefficients, matching the number of nodal points used, enforcing the collocation condition suffices to determine the interpolation weights uniquely. The consistency constraint is also satisfied. The scheme is well known to be second-order accurate, i.e., the magnitude of the interpolation error decreases asymptotically as (Δx^2) as the grid spacing tends to zero. It is C^0 continous because of the piecewise linear nature of the approximating function.

Figure 4.1 shows a spherical particle in a cubic cell and, referring to the indices shown in this figure, the approximation $\mathbf{v}$ for the velocity field is obtained by calculating:

$$\mathbf{v}(x,y,z,t) = \sum_{n=i}^{i+1} \sum_{m=j}^{j+1} \sum_{l=k}^{k+1} \mathbf{u}(n,m,k) P_n(x) P_m(y) P_l(z), \tag{4.2}$$

The form of the basis functions for a two-dimensional interpolation (figure 4.2) is given by:

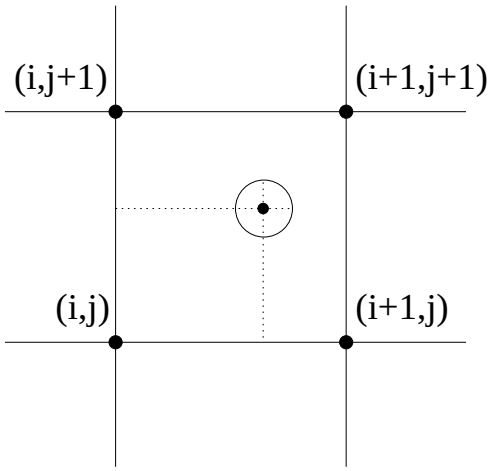

Fig. 4.2. Particle in a two-dimensional cell

$$P_i(x) = \frac{x - x_{i+1}}{x_i - x_{i+1}}, \qquad P_{i+1}(x) = \frac{x - x_i}{x_{i+1} - x_i} \tag{4.3}$$

$$P_j(y) = \frac{y - y_{j+1}}{y_j - y_{j+1}} \qquad P_{j+1}(y) = \frac{y - y_j}{y_{j+1} - y_j} \tag{4.4}$$

so the final result for $\mathbf{v}$ is

$$\begin{aligned} \mathbf{v} = {} & u_{i,j} P_i(x) P_j(y) + u_{i,j+1} P_i(x) P_{j+1}(y) \\ & + u_{i+1,j} P_{i+1}(x) P_j(y) + u_{i+1,j+1} P_{i+1}(x) P_{j+1}(y) \end{aligned} \tag{4.5}$$

the extension to the 3-D case can be obtained by using the eq.4.2 considering the basis function in z direction.

As we have already pointed out, this method is very useful because its implementation is straightforward and gives good results despite its formal poor accuracy with respect to other schemes.

4.2.2 Lagrange Polynomials

In order to increase the accuracy of the interpolation procedure one can choose to use a polynomial interpolation. This implies a more complex numerical procedure. In general, a m^{th} order Lagrangian interpolation involves $m + 1$ data points; the interpolation formula is given by:

$$\mathbf{v}(x, y, z, t) = \sum_{i=1}^{m+1} \sum_{j=1}^{m+1} \sum_{k=1}^{m+1} \mathbf{u}(i, j, k) L_i(x) L_j(y) L_k(z), \tag{4.6}$$

where the Lagrange polynomials L_i, L_j and L_k, are given by:

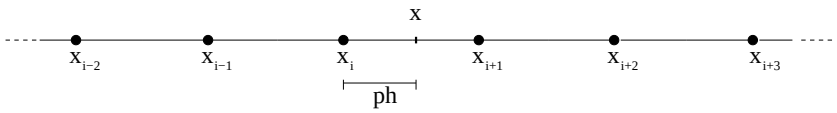

Fig. 4.3. Local coordinate in a regular cartesian grid

$$
\begin{aligned}
L_i(x) &= \prod_{n=1;n\neq i}^{m+1} \frac{x - x_n}{x_i - x_n} = \begin{cases} 1 & \text{if } x = x_i, \\ 0 & \text{if } x = x_n; n \neq i \end{cases} \\
L_j(y) &= \prod_{n=1;n\neq j}^{m+1} \frac{y - y_n}{y_j - y_n} = \begin{cases} 1 & \text{if } y = y_j, \\ 0 & \text{if } y = y_n; n \neq i \end{cases} \\
L_k(z) &= \prod_{n=1;n\neq k}^{m+1} \frac{z - z_n}{z_k - z_n} = \begin{cases} 1 & \text{if } z = z_k, \\ 0 & \text{if } z = z_n; n \neq i \end{cases}
\end{aligned}
\tag{4.7}
$$

In a one-dimensional context this interpolation scheme approximates the value of some function $f(x)$ by the series:

$$f(x) \approx \sum_{i=1}^{m+1} f(i) L_i(x)$$

The scheme uses the function values at the $(m+1)/2$ grid points lying either side of the particle position to fit a polynomial of degree m through these $m+1$ nodal values. As the grid spacing Δx goes to zero, the error of the approximation decreases as $O(\Delta x^{m+1})$ (see Balachandar & Maxey (1989)).

In the case of a regular grid in which the grid points are equally spaced (i.e. Δx uniform over the mesh) it can be useful to define a local coordinate and evaluate the polynomials with respect to such local coordinate. We consider a set of points in the neighbourhood of the point x in which we want to interpolate the grid point values (figure 4.3). In the specific case of a 2^{th} order polynomial we will consider the points x_i, x_{i+1}, for a 4^{th} order the points x_{i-1}, x_i, x_{i+1}, x_{i+2} and so on. If we put $h = \Delta x$ we can thus define:

$$p = \frac{x - x_i}{h} \tag{4.8}$$

From this definition follows for example:

$$
\begin{aligned}
x_{i-1} &= x - h(1+p) \\
x_i &= x - ph \\
x_{i+1} &= x + h(1-p) \\
x_{i+2} &= x + h(2-p)
\end{aligned}
$$

In the case of order 4 Lagrange polynomial interpolation we ca calculate the coefficients:

$$\begin{aligned} L_{i-1} &= \frac{x-x_i}{x_{i-1}-x_i}\frac{x-x_{i+1}}{x_{i-1}-x_{i+1}}\frac{x-x_{i+2}}{x_{i-1}-x_{i+2}} \\ &= \frac{hp}{-h}\frac{-h(1-p)}{-2h}\frac{-h(2-p)}{-3h} \\ &= \frac{(1-p^2)(2-p)}{6} \end{aligned}$$

$$\begin{aligned} L_{i} &= \frac{x-x_{i-1}}{x_{i}-x_{i-1}}\frac{x-x_{i+1}}{x_{i}-x_{i+1}}\frac{x-x_{i+2}}{x_{i}-x_{i+2}} \\ &= \frac{h(1+p)}{h}\frac{-h(1-p)}{-h}\frac{-h(2-p)}{-2h} \\ &= \frac{(1-p^2)(2-p)}{2} \end{aligned}$$

$$\begin{aligned} L_{i+1} &= \frac{x-x_{i-1}}{x_{i+1}-x_{i-1}}\frac{x-x_{i}}{x_{i+1}-x_{i}}\frac{x-x_{i+2}}{x_{i+1}-x_{i+2}} \\ &= \frac{h(1+p}{2h}\frac{ph}{h}\frac{-h(2-p)}{-h} \\ &= \frac{-p(p+1)(p-2)}{2} \end{aligned}$$

$$\begin{aligned} L_{i+2} &= \frac{x-x_{i-1}}{x_{i+2}-x_{i-1}}\frac{x-x_{i}}{x_{i+2}-x_{i}}\frac{x-x_{i+1}}{x_{i+2}-x_{i+1}} \\ &= \frac{h(1+p)}{3h}\frac{ph}{2h}\frac{-h(1-p)}{h} \\ &= \frac{-p(1-p^2)}{2} \end{aligned}$$

This form of the coefficients can be very useful and can be easily implemented in a routine. Similar expression can be found for higher order polynomials, keeping in mind that for lagrangian particle tracking the higher order used is commonly the 6^{th}.

4.2.3 Cubic Spline

Both linear and Lagrangian interpolation provide a continuous interpolating function in across the sub-intervals considered. Nonetheless, the problem is that the derivative of such interpolated function is not continuous across the sub-interval boundaries. In order to overcome the discontinuity in the slope of the interpolating function with linear and Lagrangian interpolation cubic

splines are used. The essential idea behind cubic spline interpolation is to fit a set of discrete data with a piecewise function of the form:

$$S(x) = \begin{cases} s_1(x) & x_1 \leq x \leq x_2 \\ s_2(x) & x_2 \leq x \leq x_3 \\ & \vdots \\ s_{n-1}(x) & x_{n-1} \leq x \leq x_n \end{cases} \tag{4.9}$$

Each function s_i is a third degree polynomial defined by:

$$s_i(x) = a_i(x - x_i)^3 + b_i(x - x_i)^2 + c_i(x - x_i) + d_i \tag{4.10}$$

These basis functions are constructed as piecewise cubic that are continously differentiable. Thus, the function $S(x)$ will interpolate all data points and will be C^2. The constraints that need to be applied to determine the coefficients in eq.4.10 are:

1. Continuity of $S(x)$: $s_i(x_i) = s_{i-1}(x_i)$
2. Continuity of $S^{'}(x)$: $s_i^{'}(x_i) = s_{i-1}^{'}(x_i)$
3. Continuity of $S^{''}(x)$: $s_i^{''}(x_i) = s_{i-1}^{''}(x_i)$

By introducing $E_i = s_i^{''}(x_i)$ we can calculate the coefficients, for a given interval in the case of an equispaced grid so that $\Delta_x = x_i - x_{i-1}$; it can be easily verified that:

Put $S(x_i) = y_i$ for $i = 1, \cdots, n-1$; since $x_i \in [x_i, x_{i+1}]$, $S(x_i) = s_i(x_i)$ then $y_i = s_i(x_i) \Rightarrow y_i = d_i$ for $i = 1, \cdots, n-1$. From the continuity constraint we have that:

$$s_i(x_i) = s_{i-1}(x_i), \qquad i = 2, \cdots, n-1$$

and

$$s_{i-1}(x_i) = a_{i-1}(x_i - x_{i-1})^3 + b_{i-1}(x_i - x_{i-1})^2 + c_{i-1}(x_i - x_{i-1}) + d_{i-1}$$

then if we put $h = x_i - x_{i-1}$ we can write:

$$d_i = a_{i-1}h^3 + b_{i-1}h^2 + c_{i-1}h + d_{i-1} \tag{4.11}$$

From the second constraint we have:

$$s_i^{'}(x_i) = s_{i-1}^{'}(x_i), \qquad i = 2, \cdots, n-1$$

We have:

$$s_i^{'}(x_i) = c_i$$

and

$$s_{i-1}^{'}(x_i) = 3a_{i-1}(x_i - x_{i-1})^2 + 2b_{i-1}(x_i - x_{i-1}) + c_{i-1}$$

then:

$$c_i = 3a_{i-1}h^2 + 2b_{i-1}h + c_{i-1} \tag{4.12}$$

For the second derivative we have:

$$s_i^{''}(x) = 6a_i(x - x_i) + 2b_i$$

from which:

$$s_i^{''}(x_i) = 2b_i$$

Then from the condition on the second derivatives of the piecewise polynomial:

$$s_{i+1}^{''}(x_{i+1}) = s_i^{''}(x_{i+1}) \qquad i = 1, \cdots, n-2$$

So that:

$$2b_{i+1} = 6a_ih + 2b_i$$

Put $E_i = s_i^{''}(x_i)$ and express the equations in terms of E_i.

- Since $s_i^{''}(x_i) = 2b_i = E_i$ then.

$$b_i = \frac{E_i}{2} \tag{4.13}$$

-

$$d_i = y_i \tag{4.14}$$

- Since $2b_{i+1} = 6a_ih + 2b_i$ and from4.13:

$$a_i = \frac{E_{i+1} - E_i}{6h} \tag{4.15}$$

- From eq.4.11 we can obtain c_i:

$$c_i = \frac{-a_ih^3 - b_ih^2 - d_i + d_{i+1}}{h}$$

substituting a_i,a_{i+1} from eq.4.15 and with trivial algebra:

$$c_i = \frac{y_{i+1} - y_i}{h} - \left(\frac{E_{i+1} + 2E_i}{6}\right)h \tag{4.16}$$

If we put $h = \Delta_x$ and $S(x_i) = y_i$ we have determined the equations:

$$\begin{cases} a_i = \frac{E_{i+1} - E_i}{6\Delta_x} \\ b_i = \frac{E_i}{2} \\ c_i = \frac{S(x_{i+1}) - S(x_i)}{\Delta_x} - (\frac{E_{i+1} + 2E_i}{6})\Delta_x \\ d_i = S(x_i) \end{cases} \tag{4.17}$$

With these substitutions we obtain a tridiagonal system; in a compact form we have:

$$\sum_{j=1}^{N} T_{ij} E_j = \frac{6}{\Delta_x^2} \left(S(x_i) - 2S(x_{i+1}) + S(x_i) \right), \qquad (i = 1, ..., N-2) \tag{4.18}$$

The system has $N-2$ rows and N columns and is under-determined. Two other conditions are required in order to solve the system and generate a unique cubic spline. In the case of a natural spline it is necessary to put to zero the first and the last unknown; that means to impose zero values for the second derivatives at the endpoints:

$$E_1 = E_N = 0. \tag{4.19}$$

Thus, the first and last columns of the matrix $\mathbf{T}$ can be eliminated and then the spline will be unique; the final form of the matrix will be the following:

$$\mathbf{T} = \begin{bmatrix} 4\ 1\ 0\ \ldots\ 0\ 0\ 0 \\ 1\ 4\ 1\ \ldots\ 0\ 0\ 0 \\ 0\ 1\ 4\ \ldots\ 0\ 0\ 0 \\ \vdots\ \vdots\ \vdots\ \ddots\ \vdots\ \vdots\ \vdots \\ 0\ 0\ 0\ \ldots\ 4\ 1\ 0 \\ 0\ 0\ 0\ \ldots\ 1\ 4\ 1 \\ 0\ 0\ 0\ \ldots\ 0\ 1\ 4 \end{bmatrix}. \tag{4.20}$$

With the Thomas' triangularization algorithm (Fletcher, pag.80) the system can be easily solved. Other hypotheses on the endpoints second derivatives can be made in order to obtain a unique spline; for example Yeung and Pope (1988) applied periodicity. The cubic spline is formally fourth-order accurate ($O(\Delta_x)$).

These results can be generalized for a three-dimensional interpolation (Yeung and Pope (1988)):

$$\mathbf{v}(x, y, z, t) = \sum_{k=0}^{N_b-1} \sum_{j=0}^{N_b-1} \sum_{i=0}^{N_b-1} b_i(x) c_j(y) d_k(z) e_{ijk}, \tag{4.21}$$

where $b_i(x)$, $c_j(y)$, $d_k(z)$ are the one-dimensional basis function and e_{ijk} are the basis function coefficients that can be calculated by forming a sequence of $3N_b^2$ one-dimensional splines where $N_b = N + 3$ is the number of the basis functions centered at the nodes. For a more detailed description of the basis functions the reader can refer to Yeung and Pope (1988).

4.2.4 Partial Hermite Interpolation

Balachandar & Maxey (1989) proposed a combined scheme in which for the y and z directions is used Hermite interpolation and direct summation with spectral coefficients in the last direction x. This scheme can be applied to interpolate velocities data bases from spectral simulations. For a one-dimensional case the N^{th} Hermite interpolation approximates the function $f(x)$ by:

$$\mathbf{h_n}(x) = \sum_{i=0}^{N} [f(x_i)H_i(x) + f^{'}(x_i)\bar{H}_i(x)] \tag{4.22}$$

where H_i and $\bar{H}_i$ are the basis functions that are given by:

$$H_i(x) = [1 - 2l_i^{'}(x_i)(x - x_i)][l_i(x)]^2 \tag{4.23}$$

$$\bar{H}_i(x) = (x - x_i)[l_i(x)]^2 \tag{4.24}$$

for which:

$$l_i(x) = \frac{(x - x_1)\cdots(x - x_{i-1})(x - x_{i-1})\cdots(x - x_n)}{(x - x_1)\cdots(x_i - x_{i-1})(x_i - x_{i-1})\cdots(x_i - x_n)} \tag{4.25}$$

For instance a cubic Hermite polynomial approximation can be given by:

$$h_2(x) = [1 + 2\frac{x - x_{i-1}}{x_i - x_{i-1}}][\frac{x_i - x}{x_i - x_{i-1}}]^2 f(x_{i-1}) + [1 + 2\frac{x_i - x}{x_i - x_{i-1}}][\frac{x - x_{i-1}}{x_i - x_{i-1}}]^2 f(x_i) + \frac{(x - x_{i-1})^2(x_i - x)}{(x_i - x_{i-1})^2} f^{'}(x_{i-1}) - \frac{(x - x_{i-1})(x_i - x)^2}{(x_i - x_{i-1})^2} f^{'}(x_i) \tag{4.26}$$

In this case the approximation is calculated for a point x in the interval (x_{i-1}, x_i) and asymptotically as the grid spacing Δ_x goes to zero the approximation error decreases as $O(\Delta_x^4)$.

4.2.5 Lagrange-Chebyshev

Combined scheme can be useful even if their usage can be restricted only for particular problems. Kontomaris et al.(1992) used, for their particle lagrangian tracking in turbulent channel flow, an interpolation scheme that employs Lagrange polynomials of order 6 in the homogeneous directions of the channel and Chebyshev polynomials in the inhomogeneous normal (i.e. wall normal) direction. The reader can refer to 4.2.2 for the Lagrange polynomials. The Chebyshev approximation of function $f(x)$ in the interval [-1;1] is given:

$$c(x) = (\sum_{k=1}^{N} C_k T_{k-1}(x)) - 1/2C_1 \tag{4.27}$$

where the C_k and $T_{k-1}(x)$ are the Chebyshev coefficients and polynomials respectively. For $i \geq 1$:

$$T_0(x) = 1$$

$$T_1(x) = x$$

$$T_2(x) = 2x^2 - 1$$

$$T_3(x) = 4x^3 - 3x \tag{4.31}$$

$$T_4(x) = 8x^4 - 8x^2 + 1$$

$$\dots$$

$$T_{i+1}(x) = 2xT_i(x) - T_{i-1}(x)$$

The coefficients can be calculated by:

$$C_j = \frac{2}{N}\sum_{k=1}^{N} f\left[cos\left(\frac{\pi(k-\frac{1}{2})}{N}\right)\right] cos\left(\frac{\pi(j-1)(k-\frac{1}{2})}{N}\right) \tag{4.35}$$

For a more detailed description of the Chebyshev approximation the reader can refer to the book of Press et al.(1986).

4.3 Examples

1. Lagrange interpolation of order 4, 6 of function $sin(x)$. Consider the interval between 0 and 2π and subdivide it into 8 intervals of length $\pi/4$. The function values are known in correspondence of these points. The interpolated function is shown in fig.4.4*a*. The error decreases as the order of the interpolating polynomials grow (fig.4.4*b*).

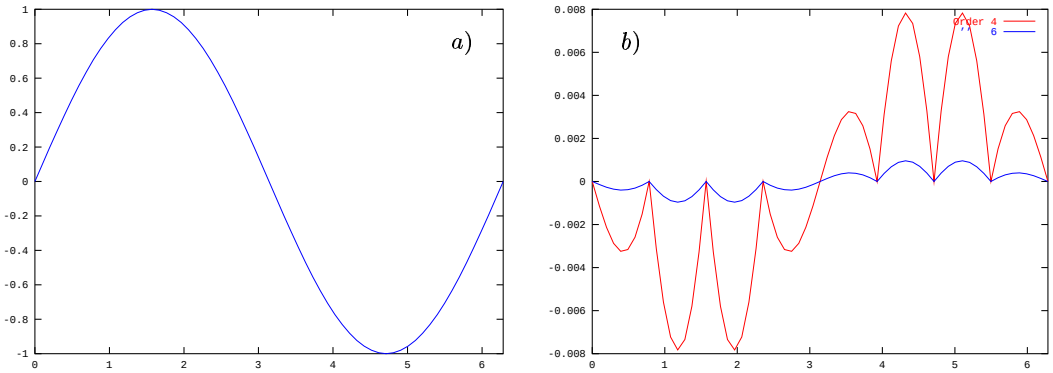

Fig. 4.4. Lagrange polynomial interpolation of order 6 of function $sin(x)$ *a*); comparison of the interpolation error between interpolating polynomials of order 4 and 6 *b*).

2. Lagrange interpolation of order 4, 6 of function $\frac{1}{1+20x^2}$. The interval $[-1, 1]$ is subdivided in 20 intervals of length 1. As in the previous example the function values are known in correspondence of these points. Fig.4.5*a* shows the resulting 6 order interpolation and as one expects the approximation improves increasing the order (fig.4.5*b*).

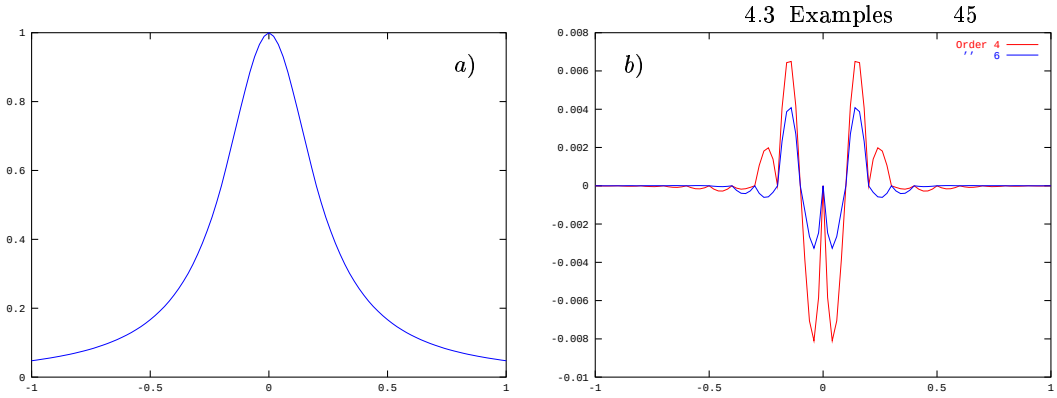

Fig. 4.5. Lagrange polynomial interpolation of order 6 of function $\frac{1}{1+20x^2}$ a); comparison of the interpolation error between interpolating polynomials of order 4 and 6 b).

---

3. Consider the function:

$$y = (1 + sin(\pi x)e^{-2x} \tag{4.36}$$

defined in the interval $[0; 1]$. We interpolate the function in the corresponding interval using lagrange interpolation of order 2 (linear), 4 and 6. Fig.4.6a shows the interpolated function and the comparison between the 3 schemes is shown in 4.6b. As the order increase the error decreases; the error decreases as the grid spacing Δ_x decreases.

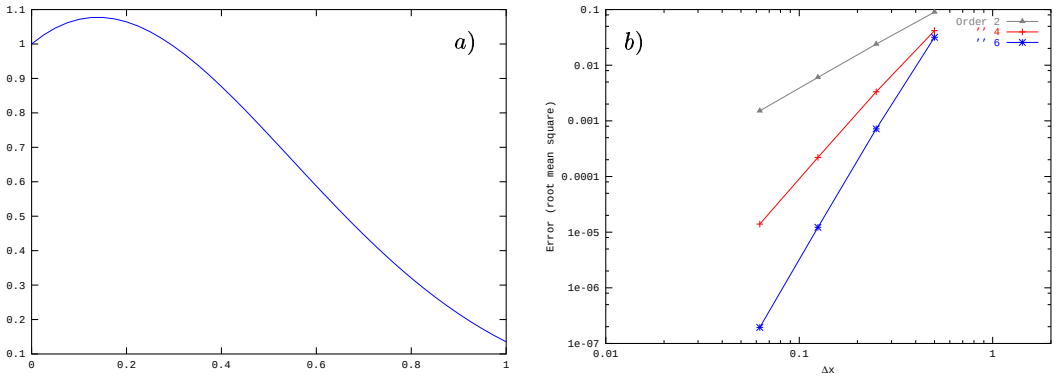

Fig. 4.6. Lagrange interpolation of order 6 of the function $(1 + sin(\pi x)e^{-2x}$ with grid spacing 6.25^{-2} a); root mean square error for lagrange interpolation of order 2, 4 and 6 as function of the grid spacing b).

---

4. Consider the $sin(x)$ fucntion of example 1. Use cubic spline interpolation to trace the fucntion in the same interval as above and consider 4, 8 and

16 intervals and compute the root mean square error for the 3 different grids. Fig.4.7a shows the function interpolated by a 9 point grid; the root mean square error in fig.4.7b increases with $O(\Delta_x^4)$. Is the same for the function of example 3?

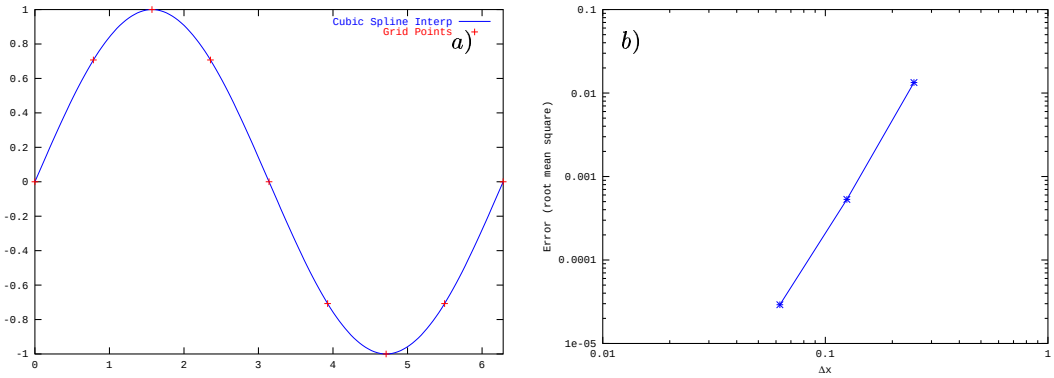

Fig. 4.7. Cubic spline interpolation of $sin(x)$ with 8 equispaced intervals, plotted with the grid points, a; root mean square error as function of the grid spacing, b.

5

Lagrangian Methods for Eulerian flow fields from: DNS, LES, RANS

Your text goes here. Separate text sections with the standard LaTeX sectioning commands.

5.1 Tracking in DNS fields

5.1.1 FD

5.1.2 Spectral

5.2 Tracking in LES fields

5.2.1 Subgrid Models

5.3 Tracking in RANS fields

5.3.1 Generalities

In the Lagrangian approach, the simulation of turbulent dispersed flow relies on the accurate characterization of turbulence in the base flow. In many applications, it is not possible to resolve the flow up to the smallest length and time scales which have effect on turbulent transport, and the effect of turbulence is to be modeled to some degree. Two widely used approaches to reproduce the effect of turbulent fluctuations in the flow on particle dispersion are:

1. eddy interaction models;
2. stochastic models.

The fist is widely used for its conceptual simplicity, because it relies on length, time and velocity scales of turbulence only to reconstruct the effect of turbulence on particle dispersion. On the other side, stochastic models base on temporal (Lagrangian) or spatial (Eulerian) autocorrelation function for velocity to reconstruct the effect of turbulence on particle dispersion. The two approaches are briefly outlined in the following.

5.3.2 Eddy interaction model

The idea behind eddy interaction models is that motion of a dispersed particulate phase is determined by particle interaction with a succession of eddies. A sketch of the flow is shown in Figure 5.1.

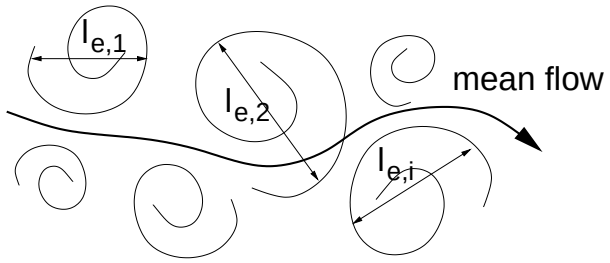

Fig. 5.1. Succession of eddies in a turbulent flow. Each eddy is characterized by a length and life-time.

Each eddy is characterized by an eddy length, l_e, and an eddy life-time, t_e, and moves at the mean velocity of the flow. Furthermore, it is assumed that turbulence contributes within each eddy with a fluctuation in eddy velocity, which remains constant for a finite time equal to t_e. Therefore, the instantaneous fluid velocity experienced by a particle crossing the eddy is given by:

$$u_e = U + u'_e \tag{5.1}$$

where U is the mean flow velocity and u'_e is the eddy fluctuation. In order to reconstruct a flow with the same characteristic of the base flow, the amplitude of the eddy velocity fluctuation u'_e is calculated as a normally distributed, random variable with zero mean and deviation equal to the RMS of fluid velocity fluctuations, $N(0, u')$.

When particles are dispersed in the flow, they move according to the mean flow field and local fluctuations generated by each eddy. In Figure 5.2 is sketched the interaction between particles and eddies.

Considering only inertia and drag and assuming Stokes regime, particle motion is described by the equation:

$$\frac{\mathrm{d}v_p}{\mathrm{d}t} = \frac{u_e - v_p}{\tau_p} \tag{5.2}$$

where v_p is particle velocity, u_e is instantaneous fluid velocity and $\tau_p = \rho_p D_p^2 / 18\mu$ is the particle characteristic time. Within each eddy, u_e is constant and the equation can be analitically integrated from $t = t_1$ to a generic t to give

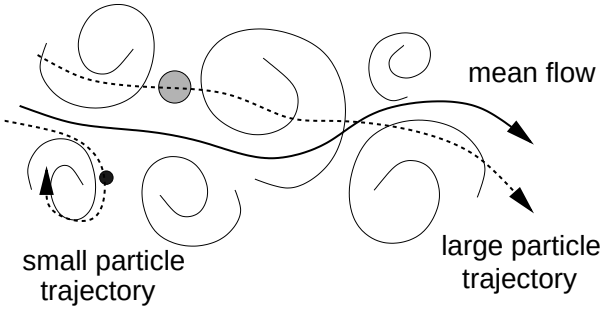

Fig. 5.2. Interaction between particles and eddies.

$$u_r = v_p(t) - u_e = -(u_e - v_p(t_1)) \exp(-t/\tau_p) \tag{5.3}$$

where u_r is the relative velocity between the eddy and the particle. The relative movement is then given by integrating Equation 5.3 once, obtaining:

$$x_r(t) = x_p(t) - u_e \cdot t = -(u_e - v_p(t_1))\tau_p \left(1 - \exp(-t/\tau_p)\right) \tag{5.4}$$

Using Equation 5.3, we can evaluate the time a particle interact with an eddy. We can identify two possibilities:

1. if the particle stopping distance is less than the eddy length, $|u_r|\tau_p < l_e$, the particle is captured by the eddy and interacts with it until it dies out. In this condition, the time of interaction is equal to the eddy life-time, $t_i = t_e$;
2. if the particle stopping distance is larger than the eddy length, $|u_r|\tau_p > l_e$, the particle spend a finite time within the eddy, leaving the eddy when the relative distance between particle and eddy equals the eddy length. The particle crossing time can be calculated as

$$x_r(t) = l_e \quad \rightarrow \quad t_c = \tau_p \ln\left(\frac{u_r\tau_p}{u_r\tau_p - l_e}\right) \tag{5.5}$$

and the eddy interaction time will be the minimum between the eddy life-time and the time for crossing, $t_i = \min(t_c, t_e)$.

For the practical implementation of the method, we need:

- the mean flow, U, and the RMS of fluid velocity fluctuations, u';
- suitable values for the eddy length, l_e, and the eddy life-time, t_e.

The selection of l_e and t_e is discussed in the next paragraph. Generally, l_e and t_e may be a function of position in the computational domain, similarly to the RMS of fluid velocity fluctuations. Given these information, the procedure to track fluid particles in the turbulent flow is as follows:

1. given the starting position for the particle, evaluate the local value for the eddy length, the eddy life-time and the RMS of fluid velocity;
2. calculate the interaction time t_i:
   a) calculate the stopping distance $|u_r|\tau_p$ and compare to the eddy length l_e;
   b) if $|u_r|\tau_p < l_e \quad \rightarrow \quad t_i = t_e$;
   c) if $|u_r|\tau_p > l_e$, calculate the crossing time from Equation 5.5 and fix $t_i = \min(t_c, t_e)$;
3. integrate Equation 5.3 and 5.4 to get the new velocity and position of the particle at the end of the interaction with the eddy;
4. consider the next eddy corresponding to the updated particle position.

5.3.3 Eddy life-time and eddy length scale

The selection of suitable values for t_e and l_e is the crucial point for the successful implementation of eddy interaction models. Among the different models proposed for l_e and t_e, we consider here the model by Gosman and Joannides (1981), which assumes that the eddy length and and life-time are equal to the dissipation scales given by

$$L_e = C_\mu^{3/4} \frac{k^{3/2}}{\epsilon} \text{ and } T_e = \sqrt{3/2} C_\mu^{3/4} \frac{k}{\epsilon} \tag{5.6}$$

where k is the turbulent kinetic energy and ϵ its rate of dissipation iand C_μ is aconstant of the $k-\epsilon$ model. In this model, the eddy length and life-time are a deterministic function of space. Other models consider l_e and t_e non deterministic values but rather randon generated variables from known probability distributions. For example, Graham and James (1996) considered l_e and t_e random variables drawn from exponential probability distributions, $f(t_e) = \exp(-t_e/T)/T$ and $p(l_e) = \exp(-l_e/L)/L$, where T and L are mean values of the distributions. In both cases, it is desiderable that reconstructed effect of turbulence is consistent with the underlying flow field.

A fist way to check consistency is to evaluate the long term dispersion obtained for fluid particles compared to the turbulent dispersion of the fluid. Wang and Stock (1992) and Graham and James (1996) have shown that a precise relation should exist between t_e and the quantities T_e and T used to define its values in order to reproduce correctly the long term dispersion for fluid particles as expected from turbulencec analysis.

Specifically, the eddy life time distribution, which may be considered as the fluid particle interaction time distribution, is related to the Lagrangian fluid velocity autocorrelation function by:

$$R_L(\tau) = \frac{\int_\tau^\infty (t_e - \tau) f(t_e) \mathrm{d}t_e}{\int_0^\infty t_e f(t_e) \mathrm{d}t_e} \tag{5.7}$$

and the Lagrangian fluid velocity autocorrelation function determines, in turn, the Lagrangian integral time scale, τ_L, as

$$\tau_L = \int_0^\infty R_L(\tau)\mathrm{d}\tau \tag{5.8}$$

Therefore, to be consistent with the modelling of turbulence a relation is obtained between L_e or L and τ_L.

For a constant life-time scheme, the probability distribution is a delta function, $f(t_e) = \delta(T_e - t_e)$. From Equation 5.7 it can be obtained:

$$R_L(\tau) = \begin{cases} 1 - \frac{\tau}{T_e} & \text{for } \tau < T_e \\ 0 & \text{for } \tau \geq T_e \end{cases}$$

and from Equation 5.8 we found

$$\tau_L = \int_0^{T_e} \left(1 - \frac{\tau}{T_e}\right) \mathrm{d}\tau + \int_{T_e}^\infty 0\mathrm{d}\tau = \frac{T_e}{2} \tag{5.9}$$

This suggests that, in order to predict correctly the long time dispersion of fluid particles, the deterministic eddy life-time should be twice the Lagrangian integral time scale of the fluid.

For an exponentially distributed eddy life time, the probability distribution is $f(t_e) = \exp(-t_e/T)/T$ where T is the mean value of the distribution. From Equation 5.7 it can be obtained:

$$R_L(\tau) = \exp(-\tau/T) \tag{5.10}$$

and from Equation 5.8 we found

$$\tau_L = \int_0^\infty \exp(-\tau/T)\mathrm{d}\tau = T\frac{T_e}{2} \tag{5.11}$$

Therefore, in order to predict correctly the long time dispersion of fluid particles, the exponentially distributed eddy life-time should have a mean value which is equal to the Lagrangian integral time scale of the fluid.

The same considerations apply for the eddy length scale. In this case, adeguate selection of L_e and L is necessary to reproduce correctly the gravitational settling of heavy, non fluid particles. For an heavy particlre settling with constant velocity V_s, the fluid velocity autocorrelation along the particle path is given by

$$G(\tau) = < u_f(x,t)u_f(x + \tau V_s + \epsilon(\tau), t + \tau) >= u'^2 R_f^p(\tau) \tag{5.12}$$

where $x + \tau V_s + \epsilon(\tau)$ is the position of the particle at time $t + \tau$. In the limit of very heavy particles, the turbulence can be assumed to be frozen in time and

$$G(\tau) = u'^2 R_E(\tau V_s, 0) \quad \text{and} \quad R_E(\tau V_s, 0) = R_f^p(\tau) \tag{5.13}$$

Integrating Equation 5.13 over τ,

$$\int_0^\infty R_f^p(\tau)\mathrm{d}\tau = \int_0^\infty R_E(\tau V_s, 0)\frac{\mathrm{d}x}{V_s} = \frac{\Lambda_E}{V_s} \tag{5.14}$$

where Λ_E is the Eulerian length scale of the flow.

Following the same procedure adopted for the eddy life-time, it can be shown that, to reproduce correctly the dispersion of heavy particles, for the constant eddy length scheme, L_e should be equal to $2\Lambda_E$ whereas for the exponentially random distributed length scales, L should be equal to Λ_E.

5.3.4 Limitation of eddy interaction model

Despite the popularity of the eddy interaction model, it fails in oredicting particle dispersion in three simple cases:

1. inertia effect;
2. crossing trajectory effects;
3. continuity effect;

Analytical and experimental results have shown that the dispersion of particles can increase with particle inertia (inertia effect), and can became larger than the dispersion of fluid particles in some cases. The original eddy interaction model uses the constraint that eddy/particle interaction time can never exceed the eddy life time, which corresponds to the fluid particle interaction time. Therefore, the model is unable to predict larger than fluid dispersion. The crossing trajectory effect was analyzed by Wells & Stock (1983), Wang & Stock (1992) and arises when dispersed particles move faster than the flow. In this condition, many eddies are crossed by the particle in a short time and the eddy interaction model reproduce only a reduced effect of turbulence due to the short time of interaction for each eddy. The conseguence is a decreased and anisotropic turbulent dispersion. The continuity effect (Csanady, 1963) corresponds to particle dispersion which is greater in the direction of gravitational drift than at at right angles to this direction.

Modifications to the eddy interaction models developed by Graham (1996b, 1998) allow to account correctly also for these effects. Specifically:

1. the inertia effect is catered for by specifying two different time scales for the eddy. Finite inertia particles are allowed to interact with eddies for a maximum interaction time T_{max} which may be greater than the interaction time for fluid particles t_e. In this way, the enhanced dispersion of hgh inertia particles can be predicted.
2. the crossing trajectory effect is accounted for by specifying the correct form of the eddy length and eddy life time distributions;
3. the continuity effect is modeled by allowing different interaction times in different coordinate directons. Specifically, when the drif velocity for particles is large, the interaction time is halved in directions perpendicular to the drift velocity whereas when the drift velocity of particles is small, the same interaction time is used for all directions. This choice allows to

reproduce particle dispesion coefficients which are identical in all direction for low drift, and lateral dispersion which is exactly half of the longitudinal dispersion for high drift.

References

1. Csanady, G., T., (1963), "Turbulent diffusion of particles in the atmosphere", *J. Atmos. Sci.*, **20**, 201-208.
2. Gosman, A., D., and Ioannides, E., (1981), "Aspects of computer simulation of liquid-fuelled combustors", Paper AIAAA-81-0323, *AIAAA* 19^{th} *Aerospace Sciences Mtg.*, St Louis, USA.
3. Graham, D., I., and James, P., W., (1996a), "Turbulent dispersion of particles using eddy interaction models", *Int. J. Multiphase Flow*, **22**, 157-175.
4. Graham, D., I., (1996b), "On the inertia effect in eddy interaction models", *Int. J. Multiphase Flow*, **22**, 177-184.
5. Graham, D., I., (1998), "Improved eddy interaction models with random lenght and time scales", *Int. J. Multiphase Flow*, **24**, 335-345.
6. Wang, L., P., and Stock, D., E., (1992), "Stochastic trajectory models for turbulent diffysion: Monte Carlo process versus Markov chain",*Atmos. Envir.*, **26A**, 1599-1607.
7. Wells, M., R., and Stock, D., E., (1983), "The effect of crossing trajectories on the dispersion of particles in a turbulent flow", *J. Fluid Mech.*, **136**, 31-62. (1996)

5.3.5 Stochastic models

The starting point of any Lagrangian approach is the particle equation of motion (see Maxey and Riley, 1983). The drag force, which appears in the equation and plays a dominant role in many conditions, is a function of the instantaneous fluid velocity as seen by the particle along its path, $v^*(t) = v(x_p(t))$. The main difficulty in the integration of the particle equation is given by the accurate prediction of this term in general turbulent flow. The instantaneous fluid velocity as seen by the particle appears to be a random variable, and information about this term can not be derived from Lagrangian fluid flow information since the solid and fluid particle trajectories become disengaged due to inertial and gravitational effects.

Lagrangian stochastic models, also known as random flight models, formulate the time evolution of the particle velocity in terms of stochastic differential equations. The velocity and position of a particle are assumed to evolve as a Markov process according to the Langevin equation (Thomson, 1986)

$$\mathrm{d}u_i = a_i(x,u,t)\mathrm{d}t + b_{ij}(x,u,t)\mathrm{d}W_j \tag{5.15}$$

where a and b are functions of the position x, the velocity u and time t, and the $\mathrm{d}W_j$ are incremental components of a Wiener process with mean zero

and variance $\mathrm{d}t$, each component being independent of the other components and uncorrelated in time. It is worth emphasizing that this simple relation embodies the main physical idea of the model: given the value of the fluid particle velocity at a certain time t, the velocity at the next time step, $t + \mathrm{d}t$, is evaluated as the sum of a deterministic term which represents the "memory" of the previous velocity and a random term which accounts for the acceleration fluctuations. Once the particle velocity is obtained, the particle positions are calculated from

$$\mathrm{d}x_i = u_i \mathrm{d}t \tag{5.16}$$

The key problem of Langevin particle dispersion models is to determine the functions a and b, known as the drift and diffusion terms respectively, for a particular turbulent flow field for which the Eulerian flow statistics are given. Criteria for their determination were given by Thomson (1986), the most general being that particles that are initially well mixed in position and velocity space in a turbulent flow must remain that way (the so-called well-mixed criterion).

In a homogeneous isotropic field, Langevin equation may be written in the equivalent form

$$\mathrm{d}u_i = -\frac{u_i}{\tau_i}\mathrm{d}t + \alpha^{1/2}\mathrm{d}\omega \tag{5.17}$$

where $\mathrm{d}\omega$ is a sequence of random numbers with a variance $< \mathrm{d}\omega^2 >= \mathrm{d}t$. The well-mixed criterion impose that $\alpha = 2\sigma^2/\tau$ where σ is the mean square velocity fluctuation and τ_i is the Lagrangian time scale, τ_L.

In non homogeneous field (Iliopoulos et al., 2003), Langevin equation should be corrected to account for the mean pressure gradient that exists in the fluid, which gives rise to a mean force,

$$\mathrm{d}u_2 = -\frac{u_2}{\tau_2}\mathrm{d}t + \alpha^{1/2}\mathrm{d}\omega_2 + \frac{\partial \sigma_2^2}{\partial x_2}\mathrm{d}t \tag{5.18}$$

where 2 is the direction in which non-homogeneity exists, or, in general terms

$$\mathrm{d}\left(\frac{u_i}{\sigma_i}\right) = \frac{-u_i}{\sigma_i \tau_i}\mathrm{d}t + \mathrm{d}\mu_i + \overline{A_i}\mathrm{d}t \tag{5.19}$$

where σ_i is the Eulerian root mean square of fluid velocity fluctuations, τ_i is a time scale of the fluid, $\mathrm{d}\mu_i$ is a random variable with zero mean, and $\overline{A_i}$ accounts for the non homogeneity of the turbulence field. The term $\overline{A_i}$ is calculated as

$$\overline{A_i} = \frac{\partial\left(\frac{\overline{u_2 u_i}}{\sigma_i}\right)}{\partial x_2} \tag{5.20}$$

and the random distribution of $\mathrm{d}\mu_i$, which is in general non Gaussian, is specified by its moments (see Iliopoulos and Hanratty, 1999). A non Gaussian distribution may be generated as:

$$\mathrm{d}\mu = pN(\mu_{l1}, \sigma_l^2) + (1-p)N(\mu_{l2}, \sigma_l^2) \tag{5.21}$$

where $N(\mu_{l1}, \sigma_l^2)$ and $N(\mu_{l2}, \sigma_l^2)$ are two random numbers having different mean and same deviation, and p is the probability of selecting a number from the first distribution. The parameters μ_{l1}, μ_{l2}, σ_l^2 and p are determined from the first four order moments of the random distribution which are given as a function of the flow variables (see Iliopoulos and Hanratty, 1999 or Thompson, 1984 for the complete derivation).

References

1. Iliopoulos, I., and Hanratty, T., J., (1999), "Turbulent dispersion in a non-homogeneous field", *J. Fluid Mech.*, **392**, 45-71.
2. liopoulos, I., Mito, Y., and Hanratty, T., J., (2003), "A stochastic model for solid particle dispersion in a non homogeneous turbulent field", *Int. J. Multiphase Flow*, **29**, 375-394.
3. Maxey, M., R., and Riley, J., J., (1983), "Equation of motion for a small rigid sphere in a non uniform flow", *Phys. Fluids*, **26**, 883-889.
4. Thomson, D., J., (1984), "A random walk modelling of diffusion in non-homogeneous turbulence", *Q. J. R. Met. Soc.*, **110**, 1107-1120.
5. Thomson, D., J., (1986), "Criteria for selection ofstochastic models of particle trajectories in turbulent flows", *J. Fluid Mech.*, **180**, 529-556.

6

Particle statistics to evaluate mixing behavior

6.1 Introductin

Lagrangian particle tracking calculations produce a large amount of data (particles position and velocity as a function of time). These data may be used to derive informations on mixing behavior in two ways: (i) detailed analysis of single particle paths allow to establish correlations between particle motion and fluid dynamics, giving valuable insights on fundamental mechanism controlling dispersion; (ii) particle data analysed from a statistical point of view allow to derive sinthetic parameters which are used to quantify dispersion, deposition and preferential distribution in a way which is useful for further engineering analysis. In the next sections some of the statistics which are generally used to describe mixing are analysed.

6.2 Dispersion coefficient

The dispersion coefficient is traditionally used (Taylor, 1921) to quantify the mixing behavior of particles since it is possible to establish a direct link between Lagrangian calculated quantities and Eulerian quantities. In the Eulerian approach, the spreading of species is described by the Fickian diffusion equation:

$$\frac{\mathrm{d}C}{\mathrm{d}t} = -\nabla\left(\nabla DC\right) \tag{6.1}$$

where D is the coefficient of turbulent diffusivity for species of concentration C. For species diffusing from a point source into stationary, homogeneous turbulence, the Eulerian coefficient D can be written as

$$D = \frac{\mathrm{d}}{\mathrm{d}t}\left(\frac{1}{2}\sigma_x^2\right) \tag{6.2}$$

where σ_x^2 is the Lagrangian dispersion of particles. Given a swarm of N particles, the Lagrangian dispersion coeffient is defined as

$$\sigma_x^2 =< x_i(t) \cdot x_j(t) > \tag{6.3}$$

where $x_i(t)$ is the i-th particle position and $< \bullet >$ indicates ensemble average. Equation 6.2 is a practical way to calculate turbulent diffusion of species when accurate Lagrangian data are available. For fluid particles, dispersion may be calculated from the flow field statistics. As demonstrated in Pope (1998), the turbulent diffusion can be calculated from the evolving position $X^+(t, Y)$ of fluid particles released from $Y = 0$ at $t = 0$. The evolutionary equation for particle position is

$$\frac{\partial X^+}{\partial t} = U^+ \tag{6.4}$$

where U^+ is the fluid velocity. Integrating equation 6.4 over time, particle position at generic time is given by

$$X^+(t) = \int_0^t U(t', 0)\mathrm{d}t' \tag{6.5}$$

which can be used to calculate the dispersion of fluid particles

$$< X_i^+(t) \cdot X_j^+(t) >=< \int_0^t U_i(t', 0)\mathrm{d}t' \cdot \int_0^t U_j(t'', 0)\mathrm{d}t'' >=$$

$$= \int_0^t \int_0^t < U_i(t', 0) \cdot U_j(t'', 0) > \mathrm{d}t'\mathrm{d}t'' \tag{6.7}$$

The term is square brackets is the Lagrangian velocity correlation, which can be rewritten as

$$< U_i(t', 0) \cdot U_j(t'', 0) >= u'^2 \rho(t' - t'')\delta_{ij} \tag{6.8}$$

where $\rho(t'-t'')$ is the Lagrangian velocity autocorrelation function. We obtain

$$\sigma_x^2 =< X_i^+(t) \cdot X_j^+(t) >= u'^2 \int_0^t \int_0^t \rho(t' - t'')\mathrm{d}t'\mathrm{d}t'' \tag{6.9}$$

and by variable substitution

$$\sigma_x^2 = 2u'^2 \int_0^t (t - s)\rho(s)\mathrm{d}t\mathrm{d}t'' \tag{6.10}$$

For very short times, i.e. $t \ll T_L$ where T_L is the Lagrangian time scale, $\rho(s) = \rho(0) = 1$, therefore

$$\sigma_x^2 = 2u'^2 \frac{t^2}{2} = u'^2 t^2 \quad \rightarrow \quad \sigma_x = u' t \tag{6.11}$$

This means that at short times the change in velocity is negligible, the trajectories are straight lines, and tracers spread at linear rate. For large times, i.e. $t \gg T_L$,

$$\int_0^t (t-s)\rho(s)\mathrm{d}s \simeq t\int_0^t \rho(s)\mathrm{d}s = t\cdot T_L \tag{6.12}$$

where the definition of integral Lagrangian time scale has been used. Therefore,

$$\sigma_x^2 = 2u'^2 t T_L \quad \rightarrow \quad \sigma_x = \sqrt{2u'^2 t T_L} \tag{6.13}$$

This means that at large times, the tracers spread at a less than linear rate. For large time, the relation

$$D = u'^2 T_L = \frac{\mathrm{d}}{\mathrm{d}t}\left(\frac{1}{2}\sigma_x^2\right) \tag{6.14}$$

holds and establishes the link between Eulerian and Lagrangian quantities.

The dispersion of inertial particle is different from the dispersion of fluid particles for three main reasons: (i) a mean drift velocity exists due to gravity or other body forces, (ii) particles have finite inertia at interact at a variable degree with vortical structures in the fluid (crossing trajectories effect) and (iii) dispersion is not isotropic (continuity effects). The dispersion of inertial particle is compared to the dispersion of fluid particles using the Stokes parameter, which gives a measure of the separation in trajectory between fluid particles and inertial particles. The Stokes number, St, is defined as the ratio between the particle characteristic time and a time scale characteristic of the fluid. When $St \ll 1$, inertial particles behaves exactly as fluid particles; when $St \gg 1$ inertial particles are unable to interact with the fluid, and particle dispersion is smaller than fluid dispersion; finally, when $St \simeq 1$, dispersion of solid particles may become larger than the fluid.

6.3 Deposition rate

In many applications, the motion of particles due to mean flow and turbulence effects ends with the particles reaching an interface and sticking to it. This is the case for liquid and solid droplets hitting a wall or splatting over a liquid film. In these applications, the relevant information is the rate at which solid or liquid material deposits from the flow onto the interface. Two main mechanisms can drive particle depositions: a particle may reach the wall because its velocity toward the wall is large enough to cover the relative distance (free flight deposition), or the particle may approach the wall due the diffusional velocity generated by random fluctuations. The role of these mechanisms is different depending on the inertia of particles. For larger particles, the free flight deposition prevails whereas for smaller particles the diffusional mechanism prevails.

Independently from the mechanism driving the deposition of particles, Lagrangian simulations of particles trajectories can be used to evaluate the deposition rate, which is defined as the migration velocity of species toward

the collecting interface. The rate at which particle deposit is proportional to the particle concentration N/ϕ, i.e. the number of particles N divided by the occupied volume ϕ, and the area of deposition A_d. The constant of proportionality is defined as the deposition coefficient k_d, and the depositing rate is given by

$$\dot{N} = -k_d \frac{NA_d}{\phi} \tag{6.15}$$

This definition allows to calculate the variation of N as a function of time or space in a given configuration. For particles depositing over time following equation 6.15, the number of particles in the flow at time t is obtained from the balance:

$$\frac{\mathrm{d}N(t)}{\mathrm{d}t} = -\dot{N} = -k_d \frac{NA_d}{\phi} \tag{6.16}$$

and integrating by separation of variables, if k_d is constant over time, we obtain

$$\frac{N(t)}{N_0} = \exp -\frac{4k_d t}{d_t} \tag{6.17}$$

where $d_t = 4\phi/A_d$ is the hydraulic diameter, and N_0 is the number of particles at starting time. If k_d is not constant over time,

$$\frac{N(t)}{N_0} = \exp\left(-\int_0^t \frac{4k_d}{d_t}\mathrm{d}t\right) == \exp -\frac{4k_d\overline{k_d}t}{d_t} \tag{6.18}$$

we can define a time-averaged value of the deposition coefficient $\overline{k_d}$.

If deposition occurs along a wall, from a balance on the number of particles in steady state conditions we obtain

$$0 = \frac{\mathrm{d}NA\mathrm{d}x}{\mathrm{d}t} = -\frac{\mathrm{d}UAN}{\mathrm{d}x}\mathrm{d}x - Nk_dW\mathrm{d}x \tag{6.19}$$

where A is the cross section of the flow, U is the mean flow velocity, W is the depth of the flow and $\mathrm{d}x$ is the lenght of the differential volume over which the mass balance is applied. Rearranging terms,

$$\frac{\mathrm{d}N}{\mathrm{d}x} - \frac{Nk_dW}{UA} \tag{6.20}$$

and separating variables

$$\ln\frac{N(x+\mathrm{d}x)}{N(x)} = -frack_dWUA\Delta x \tag{6.21}$$

from which we can evaluate the variation of the deposition rate along the x coordinate

$$k_d(x) = \frac{UA}{W\Delta x}\ln\frac{N(x)}{N(x+\mathrm{d}x)} \tag{6.22}$$

In the numerical evaluation of k_d, we can count the number of particles already non deposited at x and at $x+\mathrm{d}x$ and then use equation 6.22 to calculate k_d.

6.4 Preferential concentration of particles

In some applications, for example those involving chemical reactions, it is important to evaluate the degree of mixing achieved from the dispersion of species because local effect due to large or small concentration may be detrimental to the overall process. The macroscopic information used to characterize mixedness is the concentration field: a uniform concentration field corresponds to perfect mixing.

Using the Lagrangian approach, mixing is related to the dispersion of particles and the more chaotic is the flow, the more homogeeneous is considered the mixing. The concentration of species can always be derived from the number density distribution of particles, which is calculated by subdividing the control volume into sub-volumes and by counting the number of particles within each sub-volume. The choice of the reference dimension for the sub-volume is a control parameter which has effect on calculated statistics. The number density distribution can be then compared to reference statistical distributions to evaluate the degree of mixing.

The reference distribution for particles randomly distributed over a control volume is given by the Poisson distribution. Following the Poisson distribution, the probability of finding k particles within a control sub-volume is

$$f(k) = \frac{\exp(-\lambda)\lambda^k}{k} \tag{6.23}$$

where λ is the average number of particles in each sub-volume, which depends on the choice of sub-volumes dimension. In the Poisson distribution, it can be shown that the variance is exactly equal to the mean.

Comparison between the real number density distribution of particles and that expected from the Poisson distribution (with the same mean value) gives a measure of how far from perfectly random the distribution is. Specifically, the deviation from the random distribution can be evaluated as

$$D = \frac{\sigma - \sigma_{poisson}}{\lambda} \tag{6.24}$$

where σ is the deviation of the real distribution from the mean value,

$$\sigma = \left(\frac{\sum_1^{N.box} (k_i - \lambda_{real})^2}{N} \right)^{0.5} \tag{6.25}$$

and $\sigma_{poisson} = \lambda$ is the deviation of the Poisson distribution. A value of D equal to zero identifies a perfectly random distribution, because the deviation of the real and the Poisson distributions are identical. Values of D larger than zero correspond to a real deviation larger than Poisson deviation. This corresponds to unevenly distributed peaks of high and low concentrations, due to particles accumulation into preferential regions. Values of D less than 0 correspond to deviation of the real distribution lower than Poisson. For

the uniform distribution $\sigma = 0$, therefore $D < 0$ identify distributions which tend to the uniform distribution. It should be remarked here that the value calculated for D depends on the choice of the dimensions for sub-volumes. When the sub-volumes lenght scale is lower than turbulence scales, a random distribution is obtained. When the sub-volumes lenght scale is larger than the largest turbulent scale, high and low concentration regions are averaged out and again a random distribution is obtained. For sub-volume lenght scales comparable to turbulence scales, D should have a maximum. This lenght scale is the one characterizing the structures in which the particles segregate.

This mixedness indicator can be used to characterize the preferential distribution of particles whose starting concentration is uniform in the domain. This is a constraint to make the Poisson distribution an adeguate term of comparison. Particles which are non uniformly distributed at starting time require a very long time to disperse quasi randomly and to become indipendent from their starting conditions. The value of D and the lenght for which D is at maximum change as a function of the particle characteristic time. The position of the maximum should each time identifies those structures whose time scale is comparable to the particle characteristic time.

6.5 Correlation dimension

A single parameter which may be alternatively used to evaluate the degree of preferential concentration of particles is the correlation dimension. It gives a measure of the dimensionality of the sub-space in which particles are distributed. The lower the dimensionality, the larger the degree of preferential concentration for particles. In this case, the reference distribution is the uniform distribution. If we take a particle and we fix a distance r, we can count the number of particles which are within the distance r from the base particle, $N_p(r)$. If we normalize $N_p(r)$ using the total number of particlesd, we obtain the cumulative frequency function distribution of finding a particle at a distance lower than r. When the distribution is uniform in the volume, the number of particles should scale as r^3; when the distribution is uniform over a surface, the number of particles should scale as r^2 and when the distribution is uniform along a curve, the number of particles should scale as r. In real cases we can calculate the cumulative frequency function distribution of finding a particle within a given distance r chosing a base particle from the swarm, a distance r and counting ithe particles for which the distance is lower than r. In general, the function $N_p(r)$ will scale with r^ν, where ν is the correlation dimension. A simple way to calculate ν is to plot the cumulative frequency function distribution on a log-log plot. The slope of the curve gives the value of ν. However, since the calculated distribution depends on the base particles, the procedure is usually repeated for different base particles, averaging the results. Results presented in Fessler et al. (1994) indicate that the correlation dimension is a function of the Stokes number. It has a minimum for the par-

ticles for which the response time is comparable to the fluid time scale. This particles are found to segregate into specific regions of the flow, giving rise to non-homogeneous distribution.

6.6 Lyapounov exponent and fractal dimension

These are two measures of particle dispersion which are derived from dynamical system theory. The system of equations governing particle motion is

$$\frac{\mathrm{d}x_p}{\mathrm{d}t} = v_p \tag{6.26}$$

$$\frac{\mathrm{d}v_p}{\mathrm{d}t} = F(v_p, u) \tag{6.27}$$

where v_p and x_p are particle velocity and position and u is fluid velocity. This is a typical example of a dynamical system, whose behavior overr time can be analysed in term of phase-space trajectories. The Lyapounov exponent measures the spreading of neighboring orbits in the phase space and is defined as

$$\lambda = \lim_{\substack{t\to\infty \\ \Delta x\to 0}} \frac{1}{t} \ln \frac{\Delta x(x_0, t)}{\Delta x_0} \tag{6.28}$$

where Δx_0 is the starting separation in the phase space and $\Delta x(x_0, t)$ is the separation of particles after a time t. Rearranging equation 6.28, the separation at time t can be written as a function of the starting separation as $\Delta x(x_0, t) = \Delta x_0 \exp(\lambda t)$. If $\lambda > 0$ the orbit is unstable because neighboring points are diverging; if $\lambda = 0$ there is a neutral fixed orbitat (the separation distance does not vary overr time) and if $\lambda < 0$ the orbit is attractive and initially seperated points converge on the orbit. Qualitatively, the larger is the Lyapounov exponent and the more chaotic is the flow. However, there is no evidence of a precise correlation between chaotic behavior of a system and enhanced particle dispersion.

A measure which is related to the Lyapounov exponent is the fractal dimension. The dynamical system governing particle motion in 3D in made of six differential equations and six Lyapounov exponents exist to characterize its chaotic behavior. The sum of these expomnents is the average rate at which a cluster of initial conditions (given by position and velocity) expands in 6-dimensional hypervolume. For a conservative (Hamiltonian) system, this quantity is zero (by Liouville's theorem). For a dissipative system, the quantity is negative and there exists an attractor for the dynamics towards which initial conditions in the basin of attraction are drawn. If the system is chaotic, at least one of the Lyapunov exponents must be positive, and a strange attractor will exist. Following the usual convention of ordering the Lyapunov exponents from the largest (most positive) to the smallest (most negative), we conclude that the first exponent must be positive for a chaotic system.

If we let $S(D)$ represent the sum of the exponents from 1 to D where $D < 6$, then it is evident that for a strange attractor, there is some maximum integer $D = j$ for which S is positive and an integer $j + 1$ for which S is negative. The attractor must then have a fractal dimension that lies between j and j + 1. Following the Kaplan-Yorke conjecture is simply to interpolate the function $S(D)$ and evaluate the value of D for which $S = 0$. That is to say, we seek the hypothetical fractional dimension in which there is neither expansion nor contraction. The fractal dimension calculated in this way gives a measure of the dimension of the sub-space in which particles accumulate. The larger the fractal dimension, the more chaotic is the system and the more dispersion is expected for particles.

References

1. Kipphan H (2000) Handbook of printmedia. Springer, Berlin Heidelberg New York
2. Brandt J, Hein W (2001) Polymer materials in joint surgery. In: Grellmann W, Seidler S (eds) Deformation and fracture behavior of polymers. Engineering materials. Springer, Berlin Heidelberg New York
3. Che M, Grellmann W, Seidler S (1997) Appl Polym Sci 64:1079–1090
4. Ross DW (1977) Lysosomes and storage diseases. MA Thesis, Columbia University, New York